Composite Structures 185 (2018) 699–715

Contents lists available at ScienceDirect

Composite Structures

journal homepage: www.elsevier.com/locate/compstruct

Strength degradation and stress analysis of composite plates with circular, square and rectangular notches using digital image correlation

A. Khechai[a,*], A. Tati[b], B. Guerira[c], A. Guettala[a], P.M. Mohite[d]

[a] Civil Engineering Laboratory, University of Biskra, Algeria
[b] Energy Engineering and Materials Laboratory, University of Biskra, Algeria
[c] Mechanical Engineering Laboratory, University of Biskra, Algeria
[d] Department of Aerospace Engineering, Indian Institute of Technology Kanpur, 208016, India

ARTICLE INFO

Keywords:
Strain field
Stress distribution
Notch
Strength
DIC technique

ABSTRACT

The design of high performance composite structures frequently includes various shape and size discontinuities for various purposes. The zones near to these notches become critical regions under various working loading. The stress concentration factor (SCF), failure process, delamination, and tensile strength degradation of aluminum as well as in E-glass laminated plates are addressed in the current study through a combination of analytical, experimental and numerical studies using finite element (FE) modeling techniques. In the first part of the current work, a series of tensile tests on laminates with various fiber orientation angles and specimens with different notch diameter/width (D/W) ratios are designed and tested to determine the SCF and fracture mechanisms for unnotched/notched specimens. In addition, strain distribution, failure patterns and damage mechanisms of laminated plates with square and rectangular holes with rounded corners have been investigated. The specimens were manufactured from commercially available aluminum and unidirectional E-glass and Medapoxy STR resin epoxy. Digital Image Correlation (DIC) technique is used to obtain full-field surface strain measurements in notched specimens with different fiber orientations and open hole sizes, in order to show their effects on SCF, failure strength and mechanisms. The strain concentration that allowed damage initiation and failure propagation in the notched laminated plates is obtained experimentally and compared with the simulation details. Furthermore, the effect of the delamination defect around the notch that was unavoidable during hole drilling process was also discussed. In the second part of this study, the experimental data was used to verify the capability of two modified stress criterions models for predicting tensile strength for both materials under consideration. It is shown that the modified models are able to predict tensile strengths of notched samples that display different stress gradients. Compared to experimental data, the accuracy of the predicted strength is within 17%. On the other hand, the numerical outputs from finite element analysis (FEA) compare favorably with experimental results, and give a good estimation for stress distribution compared to the approximate analytical results. This experimental work will be very useful for the validation of new analytical stress calculation models, damage initiation as well as failure propagation models.

1. Introduction

Composite materials are increasingly used as structural materials in aerospace, civil and other engineering applications. Their growing use has risen because of their high specific strength/stiffness properties and improved fatigue life, when compared to the more traditional materials [1]. The increasing use of these materials has motived researchers to understand their complex behaviors, especially in the presence of open notches and damage. Laminated composite plates with various notch shapes and sizes are being extensively used in different aircraft structural elements to facilitate joining of structural parts or to provide access to the interior of the structure [2,3]. During its service life, an aircraft is always subjected to diverse structural loads. However, when these structures are subjected to various load conditions, undesirable high stress concentration, which affect their performance, is produced around these notches [4]. Over last a few decades, the development of stress concentration around openings has always been of major concern, and great efforts have been made to investigate the effect of the presence of notches on laminate strength [5]. The effect of these notches on the global behavior of structures is an important topic because it causes a significant reduction in strength and service life of the composite structures. There are a variety of methods for evaluating the

* Corresponding author.
E-mail addresses: khechai@iitk.ac.in (A. Khechai), mohite@iitk.ac.in (P.M. Mohite).

https://doi.org/10.1016/j.compstruct.2017.11.060
Received 7 July 2017; Received in revised form 13 November 2017; Accepted 21 November 2017
Available online 24 November 2017

stress concentration in composite plates due to geometrical irregularities. The stress distribution around openings can be evaluated by using computational techniques, elasticity theory and experimental stress analysis such as DIC [6]. Great efforts have been made in developing accurate analytical models to determine the stress distribution in notched composite laminates.

One of the most powerful approaches for the analytical determination of stress distribution around geometric irregularities in an infinite elastic plate is Muskhelishvili complex variable approach[7]. Using this approach [7], Ukadgaonker et al. [8–10] gave stress and moment functions for laminated composite plates with openings of different shapes under in-plane and bending loadings. On the other hand, more recent work on this problem using analytical methods include a work by Rao et al. [11]. The authors derived stress functions for generalized mapping function for square and rectangular holes in symmetric laminates under arbitrarily oriented in-plane loading using Savin's [12] basic solution for anisotropic plates. Moreover, an analytical solution is given by Rezaeepazhand et al. [13] to study the stress distribution of plates with different central cutout shape. The effect of cutout geometry, material properties and fiber orientation was studied analytically in his work. While these methods are very powerful in solving a wide variety of notched plates problems, they are complicated and must be reformulated for each type of far-field load; and also they are not able to give ideas about the strength degradation, damage locations and failure mechanisms. As a consequence, great efforts have been made in developing strength prediction models for failure analysis of notched composite laminates with different open notch sizes.

A brief review on current fracture models for assessing the residual strength has been given by [14,15]. Strength prediction methods are generally based on the Point Stress Criteria (PSC) and Average Stress Criteria (ASC) proposed by Whitney and Nuismer (WN) [16]. These failure criteria involve two parameters, the unnotched strength σ_0 and the characteristic length d_0 or a_0. Whitney et al. [16] assumed that the characteristic length is a material constant, independent of the hole radius. It is then possible to predict the strength ratio. But if the characteristic length depends on the notch radius, their [16] model needs corrections. As a result, researchers [17–19] have made some modifications in the PSC to estimate the notched tensile strength of laminates with various notch sizes. These two parameters fracture models were first modified into a three parameters notched strength criterion by Pipes et al. [20]. In their model, Pipes et al. assumed that the characteristic length as a function of the hole size to reference radius, notch sensitivity factor and exponential parameter. Kim et al. [21] extended this model and expressed the possibility of varying the notch sensitivity factor with the selection of the reference radius and considered the characteristic length is a function of hole diameter, specimen width, notch sensitivity factor and exponential parameter. On the other hand, Kannan et al. [22] made some modifications in the WN model to estimate the notched tensile strength of plates with different notch sizes. More details on the modified fracture models used in the current work, (Kim [21] and Kannan [22]), will be given in the next section.

The main purpose of this study is experimental and numerical determination of the influence of geometrical notch shape (circular, square and rectangular holes) and notch size on stress concentration as well as on strength degradation and failure mechanism in aluminum and laminated specimens subjected to tensile load. Based on the FEM [23], stress distribution in composite laminates is evaluated. More details on the developed finite element model used in the current work will be given in Section 3. The specimens were manufactured from commercially available aluminum and unidirectional E-glass and Medapoxy STR resin epoxy. The complex failure mechanisms present during the work loading stage are increased due to the presence of a stress concentration, causing a wide range of damage and effects, such as stress and strain gradients. The influence of initial delamination and micro-cracks produced by drilling operation around the open notch has been discussed. It is therefore, more desirable when performing experimental study on samples to obtain extensive full-field strain data to get the global view of the damaged zone near to the open hole. There have been a number of studies in the literature using full-field measurements to examine the mechanical response of notched composite structures under mechanical loading [24–27]. The optical technique of DIC is one of the powerful methods to obtain a full-field strain data. In this experimental work, the DIC technique [28] is used to obtain full-field surface strain measurements in notched specimens with different fiber orientation angles and open notch sizes, in order to show their effects on SCF, failure strength and damage mechanisms. However, only very few number of studies focus on the assessment of the failure mechanism and strength in laminated plates with square and rectangular holes; and their relation by the stress concentration in notched composite structures using DIC techniques. In the research works [29–33] only laminated plates with circular notches were studied.

The paper is organized as follows. The work contains two main parts with several sections. In the first part, material and specimens preparation steps and different material characterization tests are explained in detail. Then, Parametric FE models are developed and the FE formulation is given. Next to this section, stress–strain curves for notched plates are given experimentally, and failure loads for different notch shapes and sizes are also obtained and discussed in this section. The stress and strain distributions around different notch size using FEM are given. Also in this section, the DIC full-field strain measurements are also obtained, focusing on damage initiation and failure propagation around the central hole. The relation between the notch shape, damage locations and the fracture mechanisms are explained in detail. In the second part, the experimental data was used to verify the capability of two modified stress criterion models for predicting tensile strength for both materials under consideration.

2. Theory

To determine the notched tensile strength of a laminated plate containing circular hole under uniaxial tensile loading, Whitney et al. [16] suggested a two parameters model called PSC. This model is based on the approximate function of the stress distribution adjacent to the opening. PSC assumes that the failure occurs when the stress σ_y over some characteristic length d_0, away from the boundary of the discontinuity is equal to or greater than the tensile strength of the material σ_0

$$\sigma_y(x,0) = \sigma_0 \quad at \quad x = R + d_0 \tag{1}$$

where R is the hole radius. For an orthotropic plate subjected to uniform stress σ_y^{∞}, the normal stress σ_y along to the x-axis ahead of the circular hole is expressed approximately by [34] as

$$\sigma_y(x,0) = \frac{\sigma_y^{\infty}}{2[2 + (R/x)^2 + 3(R/x)^4 - (k_T^{\infty} - 3)\{5(R/x)^6 - 7(R/x)^8\}]}, x > R \tag{2}$$

where the SCF K_T^{∞} for an infinite plate can be written in the following form [35]

$$K_T^{\infty} = 1 + \sqrt{2\left(\sqrt{E_y/E_x} - \nu_{yx} + E_y/G_{yx}\right)} \tag{3}$$

where E_x, E_y, ν_{yx} and G_{yx} are the effective elastic moduli of the laminate. Note that the y-axis is oriented along the loading direction, and x-axis is oriented transverse to the loading direction. Applying the PSC model of Eq. 1 in conjunction with Eq. 2, the strength ratio can be given as

$$\frac{\sigma_{Nh}^{\infty}}{\sigma_0} = \frac{2}{[2 + A^2 + 3A^4 - (k_T^{\infty} - 3)\{5A^6 - 7A^8\}]}, \quad A = \frac{R}{(R + d_0)} \tag{4}$$

where σ_0 is the tensile strength of unnotched specimen and σ_{Nh}^{∞} is the notched strength of an infinite width plate. Based on PSC model, Whitney et al. [16] assumed that the characteristic length is a material

constant, independent of the hole radius. It is then possible to predict the strength ratio. But, if the characteristic length depends on the hole radius, Whitney's [16] model needs a correction. For predicting the correct notched strength of the composite laminate with different notch size, two modified stress criteria (MSC) are used. The first one is proposed by Kim et al. [21] and the second is suggested by Kannan et al. [22]. Kim et al. [21] modified the PSC model and proposed that the characteristic length depends on the opening radius as

$$d_0 = k^{-1}\left(\frac{2R}{W}\right)^m \tag{5}$$

In this model, d_0 is a function of the open hole diameter $2R$, plate width W, notch sensitivity factor k, and an exponential parameter m. On the other hand, Kannan et al. [22] proposed that the relationship between the fracture parameters and the characteristic length d_0 can be given as

$$\frac{\sigma_0\sqrt{\pi d_0}}{k_f} = 1-m_f\left(\frac{\sigma_{Nh}^{\infty}}{\sigma_0}\right) \tag{6}$$

In this model, the fracture parameters (k_f and m_f) are to be determined by a least squares fit to the data for d_0 and $\sigma_{Nh}^{\infty}/\sigma_0$. Since, the above models were formulated by assuming that the plate is of infinite width, a comparison between the experimental data and notched strength models requires a correction for finite width of the specimen [35]. The notched tensile strength of an infinite plate σ_{Nh}^{∞} is obtained by multiplying the experimental notched strength of a finite width plate σ_{Nh} by a correction factor K_T/K_T^{∞}, and the characteristic length is determined from the MSC using the normal stress distribution adjacent to the hole in an infinite plate [36]. Here, K_T and K_T^{∞} are the SCF for finite and infinite width orthotropic plates, which are given by [37] as

$$\frac{K_T^{\infty}}{K_T} = \frac{3(1-\beta)}{2+(1-\beta)^3} + \frac{1}{2}(\beta M)^6(k_T^{\infty}-3)\{1-(\beta M)^2\} \tag{7}$$

where

$$(\beta M)^2 = \frac{1}{2}\left\{\sqrt{1-8\left[\frac{3(1-\beta)}{2+(1-\beta)^3}-1\right]}-1\right\};\quad \beta = D/W \tag{8}$$

For any material system, the constant parameters in both fracture criteria are to be determined experimentally by testing unnotched and notched specimens.

3. Finite element formulation

A partial differential equation is a relation between a function of several variables and its partial derivatives. Many problems in physics, engineering and mathematics are modeled by one or several partial differential equations. Freefem++ [38] is a software to solve some of these equations numerically. As its name implies, it is a free software based on the FEM; it is not a package, it is an integrated product with its own high level programming language. Freefem++ has an advanced automatic mesh generator, capable of a posteriori mesh adaptation; it has a general purpose elliptic solver interfaced with fast algorithms such as the multi-frontal method UMFPACK, SuperLU. Hyperbolic and parabolic problems are solved by iterative algorithms prescribed by the user with the high level language of Freefem++. It has several triangular finite elements, including discontinuous elements [38].

Elasticity solid objects deform under the action of applied forces: a point in the solid, originally at (x,y,z) will come to (X,Y,Z) after some time. The vector $u = (u_1,u_2,u_3) = (X-x,Y-y,Z-z)$ is called the displacement. When the displacement is small and the solid is elastic, Hooke's law gives a relationship between the stress tensor $\boldsymbol{\sigma}(u) = \sigma_{ij}(\boldsymbol{u})$ and the strain tensor $\boldsymbol{\epsilon}(u) = \epsilon_{ij}(\boldsymbol{u})$.

3.1. Differential or strong form of the equations of solid mechanics

The solution of an elastic static problem of solid mechanics (the domain Ω of a solid is limited by its border Γ) is governed by partial differential equations accompanied with the formulation of the boundary and initial conditions [39].

- Static equilibrium (with $\sigma_{ij} = \sigma_{ji}$).

$$\frac{\partial\sigma_{ij}(\boldsymbol{u})}{\partial x_i} + f_j = \boldsymbol{0}\ (f_j \text{ are body forces. }) \tag{9}$$

- Constitutive law (Hook's law)

$$\sigma_{ij}(\boldsymbol{u}) = C_{ijkl}\ \epsilon_{kl} \tag{10}$$

- Static boundary conditions (traction imposed)

$$n_i\sigma_{ij}(\boldsymbol{u}) = t_j\ (\text{On } \Gamma_t) \tag{11}$$

- Kinematic boundary conditions (displacement imposed)

$$u_i = \overline{u}_i\ (\text{On } \Gamma_u) \tag{12}$$

3.2. Integral or weak form of the equilibrium equations of solid mechanics

The modeling of any physical problem leads to differential equations. This differential form is called the strong form of the limit problem. The finite element method does not solve the strong form. It addresses a mathematically equivalent form, called integral form or weak form.

The integral form of equilibrium or the weak form is

$$\int_{\Omega} C_{ijkl}\ \epsilon_{kl}\ \delta\epsilon_{ij}\ d\Omega = \int_{\Omega} f_i\ \delta u_i\ d\Omega + \int_{\Gamma} t_i\ \delta u_i\ d\Gamma\ (\text{in } \Omega \text{ and on } \Gamma) \tag{13}$$

with

$$\epsilon_{ij} = \frac{1}{2}\left(\frac{\partial u_i}{\partial x_j} + \frac{\partial u_j}{\partial x_i}\right),\ \delta\epsilon_{ij} = \frac{1}{2}\left(\frac{\partial\delta u_i}{\partial x_j} + \frac{\partial\delta u_j}{\partial x_i}\right) \tag{14}$$

In Eq. 13, ϵ_{kl} are the components of the strain field, and $\delta\epsilon_{ij}$ are the components of the virtual deformation field.

3.2.1. Isotropic material

When the displacement is small and the material is isotropic, in the stationary case the following conditions are satisfied

$$-\nabla\sigma_{ij}(\boldsymbol{u}) = f_i \tag{15}$$

$$n_i\sigma_{ij}(\boldsymbol{u}) = t_j\ (\text{if traction imposed}) \tag{16}$$

$$u_i = \overline{u}_i\ (\text{if displacement imposed}) \tag{17}$$

with

$$\sigma_{ij}(\boldsymbol{u}) = \lambda\delta_{ij}\nabla\boldsymbol{u} + 2\mu\ \epsilon_{ij}(\boldsymbol{u}) \tag{18}$$

δ_{ij} is the Kronecker delta, λ and μ are Lame's constants that describe the mechanical properties of the isotropic solid, and are themselves related to the better known constants E, Young's modulus and ν, Poisson's ratio as

$$\mu = \frac{E}{2(1+\nu)}, \lambda = \frac{\nu E}{(1+\nu)(1-2\nu)} \tag{19}$$

3.2.2. Composite material

The integral form of equilibrium or the weak form is extended to study the stress distribution in composite materials. In this formulation,

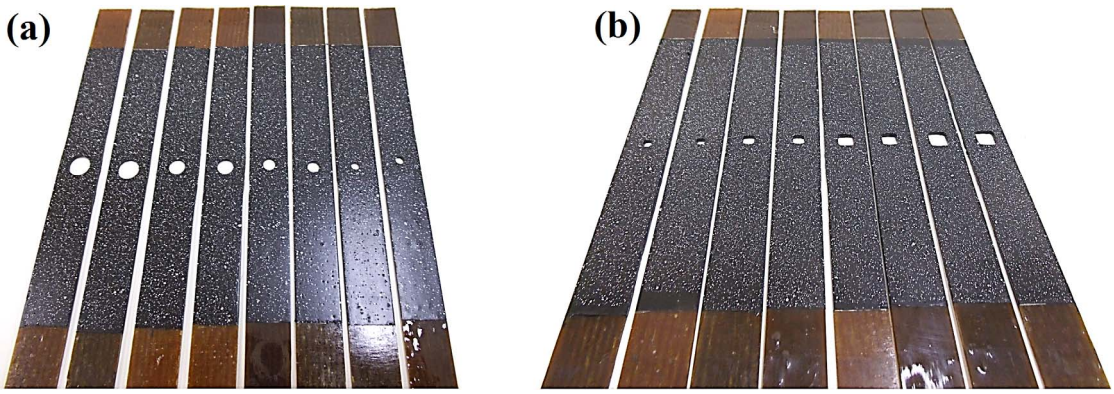

Fig. 1. Specimens with different open notches shapes and sizes (a) circular holes and (b) square holes.

the classical laminate theory is adopted in order to give the constitutive relationship between the force resultants and the strains field.

By adopting the classical laminate theory, the forces N and moments resultants M are related to the mid-surface strains ϵ^0 and to the curvatures $\boldsymbol{k}$ by

$$\begin{Bmatrix} N \\ M \end{Bmatrix} = \begin{bmatrix} A & B \\ B & D \end{bmatrix} \begin{Bmatrix} \epsilon^0 \\ k \end{Bmatrix} \tag{20}$$

where [A], [B] and [D] are the extensional, coupling and bending rigidity matrices, respectively, and are defined as

$$\{A,B,D\}^T = \int_{-h/2}^{h/2} [\overline{Q}_{ij}]_k (1,z,z^2) dz \tag{21}$$

with $\overline{Q}_{ij}$ are the stiffness coefficients of a layer in the global coordinate system (x,y,z) of the laminate forming an angle θ with the local coordinate system of the lamina. The stiffness coefficients are given by

$$\begin{aligned}
\overline{Q}_{11} &= Q_{11}c^4 + Q_{22}s^4 + 2(Q_{12} + 2Q_{66})s^2c^2 \\
\overline{Q}_{22} &= Q_{11}s^4 + Q_{22}c^4 + 2(Q_{12} + 2Q_{66})s^2c^2 \\
\overline{Q}_{12} &= (Q_{11} + Q_{22} - 4Q_{66})s^2c^2 + Q_{12}(s^4 + c^4) \\
\overline{Q}_{66} &= (Q_{11} + Q_{22} - 2Q_{12} - 2Q_{66})s^2c^2 + Q_{66}(s^4 + c^4) \\
\overline{Q}_{16} &= (Q_{11} - Q_{12} - 2Q_{66})sc^3 - (Q_{22} - Q_{12} - 2Q_{66})s^3c \\
\overline{Q}_{26} &= (Q_{11} - Q_{12} - 2Q_{66})s^3c - (Q_{22} - Q_{12} - 2Q_{66})sc^3
\end{aligned} \tag{22}$$

where $s = sin(\theta)$ and $c = cos(\theta)$.

4. Experimental procedure

In the following the procedure to prepare materials and specimens from them is explained in brief. Further, the experimental procedure is also presented in brief.

4.1. Materials and specimen preparation

During this work, specimens with different opening sizes and fiber orientation angles were fabricated by hand lay-up method. The initial materials were laid up by hand in 300 mm wide by 500 mm long plates with various fiber orientation angles. Mold release agent is first applied to the mold for getting a high-quality surfaces and facilitate the release of the laminate from the metallic mold. When the agent has cured sufficiently, the unidirectional glass fiber is manually placed on the mold. The resin is applied by brushing. A paint roller is used to consolidate the laminate, thoroughly wetting the reinforcement and removing the entrapped air. Subsequent layers of the unidirectional glass fiber are added to build the required laminate thickness. The laminates were preserved at room temperature for more than 7 days. The specimens were made of 4-ply unidirectional (UD) E-Glass/Epoxy lamina. The thickness of individual ply is 0.5 mm. The initial materials, E-glass fiber 400 g/m^2 and Medapoxy STR resin epoxy with a density of 1.15 g/cm^3 and a hardener with a density of 1.02 g/cm^3, used in the manufacturing of the specimens, were purchased from SF composites (France).

The completed laminates have been checked to ensure good quality without defects and then cut into specimens with a total length of $L = 250$ mm, a width of $W = 25$ mm, using a dedicated cutting machine with a diamond-coated blade. To create circular holes at the center of specimens, different sizes of drills were used. In order to limit the effects of delamination around the openings caused by the drilling process, wood en plates under the specimens and a drill machine with a speed of 2300 rad/min, were used to ensure that all the notched specimens had holes in similar conditions. Different sizes of drill, including (0 'un-notched', 2.5, 5, 7.5, 10, and 12.5 mm) were used to obtain different diameter to width (D/W) ratios. A circular hole is machined by initially drilling a starter hole of smaller diameter, and then carefully enlarging it to its final dimensions by incremental drilling. On the other hand, the following procedure is followed to create various sizes of square (4 × 4, 6 × 6, 8 × 8 and 10 × 10 mm^2) and rectangular (4 × 8, 6 × 12 and 8 × 16 mm^2) notches at the center of laminated specimens. The first step is to make a transparent paper and fixing it onto the laminated plate using adhesive tape. The transparent paper shows the 4 corners as well as the center of the rectangle. A needle is used to mark the center locations on the laminated plates. A straight edge and the needle are used to connect the 4 points. Initially, 1 mm diameter drill is used for creating the initial holes at the 4 points and the center. Starting with a small diameter drill improves the accuracy of the location of the hole. Then, using a drill of sufficient diameter, a bigger hole centered at the initial hole is created just to reach the edges of the square/rectangle. The small drill is also used to remove the extra material inside the square/rectangle and to get the edges of the hole closer to the drawing lines. The finishing work will be done using a flat file to get straight edges. The specimen surfaces were scrubbed and were cleaned thoroughly to remove the dirt. Before the testing, the DIC specimens were prepared and covered using a black paint and sprayed with a white aerosol to create a random speckle pattern, which was used for the DIC analysis, (see Fig. 1).

In-plane mechanical properties were measured by following ASTMD3039 [40] and ASTMD3518 [41] for tensile and shear properties, respectively. The tensile properties of the specimens, such as laminate Young's modulus E_1,E_2, Poisson's ratio ν_{12} and unnotched strength were measured by static tension testing of longitudinal $[0]_4$ and transverse $[90]_4$ unidirectional specimens under normal environment conditions (temperature 24 ± 2.5 °C, humidity 45 ± 5%). The shear modulus of the laminate was determined by loading the laminate specimens whose principal axes are on 45°. Four identical specimens were used in the material characterization tests. In addition, in order to get ideas about the fiber orientation effect on stress distribution and SCF values, plates with different fiber orientation angles (0°, 45°, −45° and 90°) were manufactured and circular hole with $D = 4$ mm was chosen to limit the hole size effect and the plate can be considered as

infinite.

As isotropic specimens, aluminum plates were prepared; and the same dimensions ($250 \times 25 \times 2\,mm^3$) and different opening sizes were considered. A typical strain rate for standard test samples is about $0.5\,min^{-1}$ for each family of test.

Remark: For DIC measurements only one surface of the specimen is painted. The thickness of the paint must be very small compared to the thickness of the specimens; otherwise the paint later will have effect on overall deformation pattern of the laminate (due to unsymmetry) being tested. Thus, ideally both surfaces must be painted. However, in the present study only one surface is painted with very thin layer and therefore, its effect on overall deformation is neglected.

Remark: Delamination is one of the main defects that we can observe during the drilling of laminated plates and can be an important limiting factor for the use of composite materials. This is because the drilling process causes micro-cracks and these cracks are the origin of the high stress concentrations. It has been observed that the lower cutting speed can minimize delamination and lead to a better notched surface. Also, wood en plate under the specimens is used in order to limit the effects of delamination around the openings caused by the drilling process. On the other hand, it has been observed that the delamination zone and the broken fibers around the notches using 2.5, 5, 7.5 mm drills are less compared to 10 and 12.5 mm drills.

4.2. Experimental setup

A universal testing machine (INSTRON-5969) was used to conduct the tests on the laminates as well as the aluminum specimens. A high precision load cell with a capacity of 10 kN is used for recording the load. The ends of the specimens were carefully mounted in the wedge grips of the machine to make sure that the specimen is aligned and centered. The specimens were loaded in tension to failure at a crosshead strain rate of $0.5\,min^{-1}$ to ensure steady deformation and recorded easily. When loading, the whole test process was carefully recorded by the force/displacement curves and final damage pictures were obtained using manual photographing. The specimen was illuminated by ordinary white light during the experiment. High resolution images during the loading event were taken using a digital camera using an appropriate speckle pattern. The experimental data obtained in this study were processed with open source 2D-DIC software[28]. Elastic deformations around the notch were evaluated using DIC method, which basically captures successive pictures throughout the load application period, thus assessing the continuous change in the specimen's surface around the notch caused by the elastic deformation. So, DIC involves comparing images of an object before and after its deformation and presenting the relevant information thus obtained in the form of pixels, which can then be converted into metric units such as necessary [42]. Fig. 2 shows the experimental test setup and a typical example of the random pattern on the surface of specimen produced by spraying paint.

To perform DIC experiments, three identical specimens were used and the results are averaged, because it is very difficult to generate a suitable pattern with manual paint. This procedure was repeated for all opening size and fiber orientation angles to obtain correct stress concentration to eliminate the error due to the speckle pattern.

5. Finite element modeling

In this study, 2D FEA was carried out using the open source FE software Freefem++ [38] with quadratic triangular element (P2), as show in Fig. 3. As it was known, 2D models have the advantage of high efficiency and less time consuming. On other hand, it is also preferable to use open source finite element modeling technique. Freefem++ is a software to solve partial differential equations numerically. The FE models of all groups of specimens, including circular holes (with different cutout size and different fiber orientation angles) as well as plates with square and rectangular notches (with different sizes as mentioned above) are created and the stress distribution around the openings is obtained. The elastic orthotropic properties used in this investigation will be given in the next section. Furthermore, in view of the rapid change in the stress field near the hole, a higher mesh density with smaller elements is adopted and coarse meshes far from the notched region are used. A convergence study is carried out to obtain initial appropriate mesh in the open notch zone. Then automatic parametric program was developed changing the open hole size, the fiber orientation angle and the mesh refinement, because if we keep the same number of elements around the cutout boundary, the stress distribution will be affected changing the hole size. The initial element numbers around the circular hole are 30 and 5 elements will add to the previous element number for each iteration. For plates with square and rectangular notches, the initial element number on each side of the notch is 60 and 10 elements will add for each iteration. The radius of the circular corner is 0.5 mm (similar to the experimental models) and it divided to 20 elements. In the analyses, the nodes on the bottom end B are fully restrained for all displacement (u,v), while the nodes on the top end A were loaded (10 MPa).

6. Results and discussion

6.1. Experimental unnotched tensile proprieties

The performed experimental tests aimed to evaluate the tensile strength of unnotched/notched specimens and determine the strain distribution in laminated plates containing different notch sizes in order to calculate the stress state. The results obtained from the longitudinal tension tests, for both materials under consideration, are summarized in Table 1. Figs. 4–7 show typical stress–strain curves for four unnotched aluminum and laminate specimens used for material characterization. The following were observations for the longitudinal tension tests.

(a) It can be seen from the figures that the curves, for each family of test, have identical behavior and the curves almost overlap each other.
(b) The stress–strain curves for aluminum and composite materials used in this study were practically superposed in the elastic region.
(c) There are three distinct regions in the behavior of both materials; the first is the initial elastic region where the behavior is essentially linear up to the (LP) point (end of the linear part of the curve). This linear elastic phase is characterized by the elastic modulus. Following this part, the curves lose relatively its linearity and start of damage, and the third one with a nonlinear increase of tensile stress with longitudinal strain up to a final rupture (final damage).
(d) Composite material shows an elbow at the end of the elastic region (LP) which can be related to an earlier fiber breakage initiation or pulling-out of fibers happened at end of the linear loading stage resulted from the poor fiber–matrix interfacial strength of these laminates.
(e) The failure positions of the most specimens were near the center. Then as expected, the damage mechanism was following the fibers direction. Some specimens were clearly failed in the end of the grips. Each family of specimens test has practically the same strength and the averaged values could be accepted as an approximation of the true material strength. The average values of the tensile strength for four unnotched composite plates are 576.92, 82.01, 37.37 MPa for $[0]_4$, $[45]_4$, $[90]_4$ laminates, respectively. The tensile strength for aluminum specimens is 160.9 MPa. The longitudinal strength of composite material is 3.6 times greater than the aluminum, but the transverse strength is reduced.

6.2. Experimental notched tensile strength degradation

The tensile strength results for the unnotched and notched

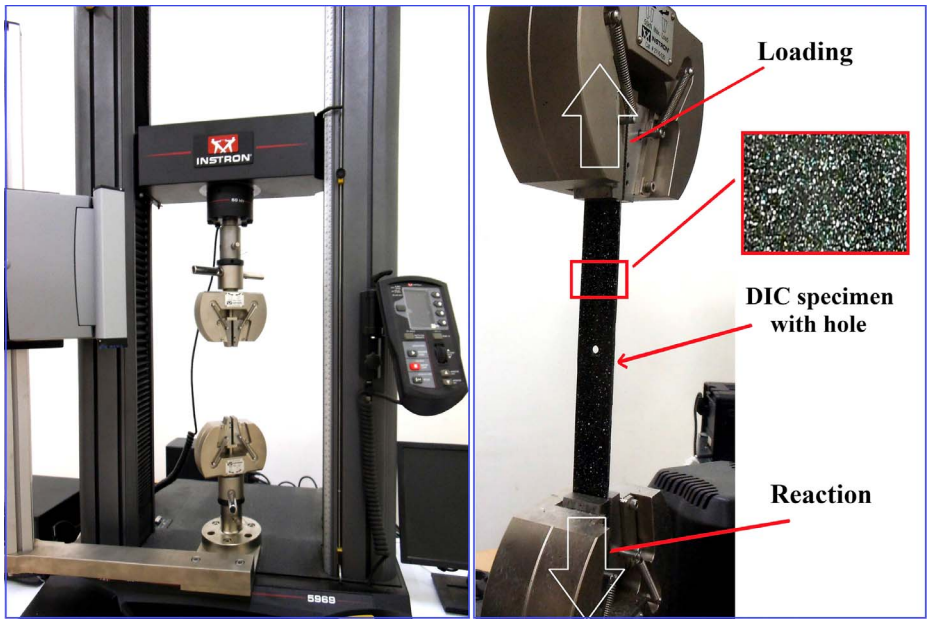

Fig. 2. Experimental setup for DIC testing.

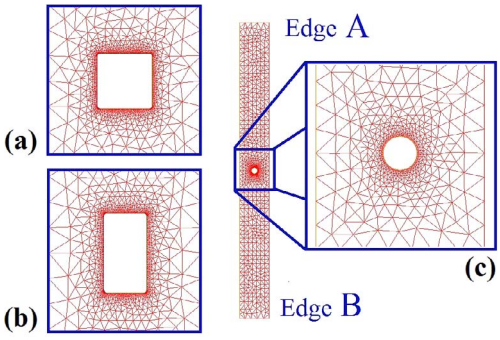

Fig. 3. Final mesh pattern of the specimen with open holes (a) square hole (b) rectangular hole and (c) circular hole.

Table 1
Material properties.

Materials	Elastic properties				Thickness
	E_1 (GPa)	E_2 (GPa)	G_{12} (GPa)	ν_{12}	h (mm)
Isotropic	23.15	23.15	9.04	0.28	2 ± 0.2
E-Glass/Epoxy	22.54	10.94	3.54	0.30	2 ± 0.3

longitudinal $[0]_4$ laminate specimens as well as for plates with different fiber orientation angles are shown in Figs. 8–11. The strength degradation of composite laminate was subsequently compared to that of aluminum specimens. Fig. 8 shows the stress-stain curves obtained experimentally and one can clearly see that the degradation of strength values was related to the circular notch diameter. The ultimate strength values varies greatly with the hole size, and the laminate strength decreases as the hole size increases. The same behavior is also shown for plates containing square (Fig. 9) and rectangular (Fig. 10) notches. From the stress–strain curves shown in the Figs. 8–10, it is noticed that plates with different shape and size of notches showed practically the same slope reduction compared to unnotched plates. This means that the Young's modulus degradation for the perforated plates is relatively the same. In addition, all the notched specimens showed a nonlinear elbow at the end of the elastic region which can be related to an earlier fiber damage initiation. Accordingly, the nonlinearity of the perforated specimens is mainly associated with the fiber damage, delamination

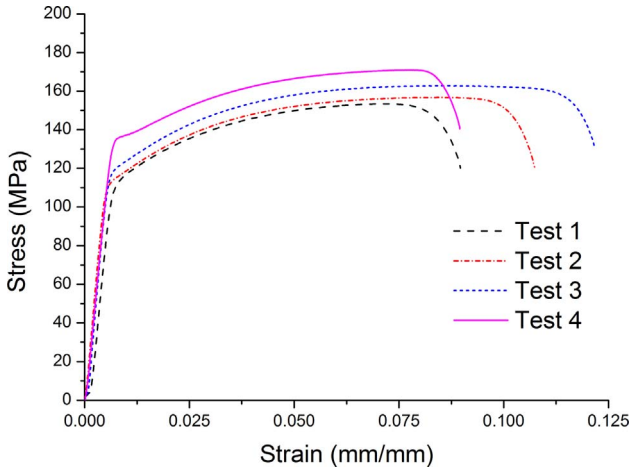

Fig. 4. Typical stress–strain curves for aluminum specimens.

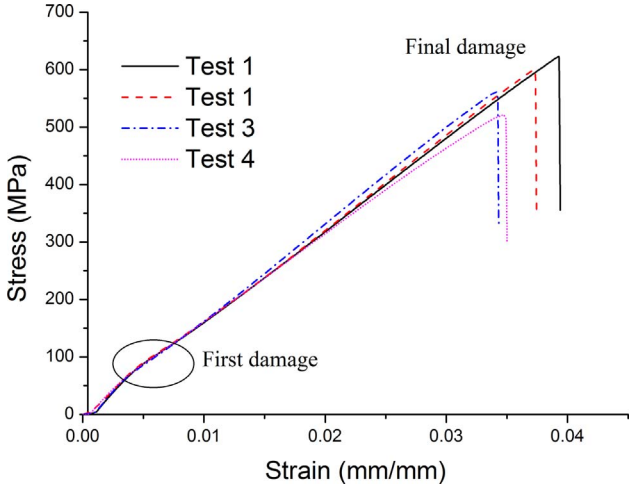

Fig. 5. Typical stress–strain curves for $[0]_4$ laminates.

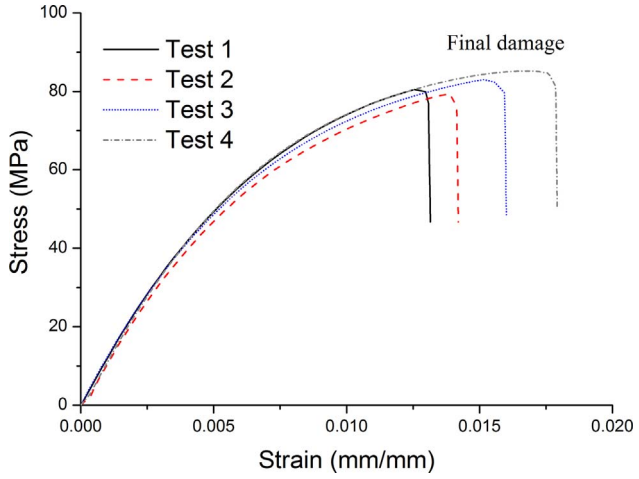

Fig. 6. Typical stress–strain curves for $[45]_4$ laminates.

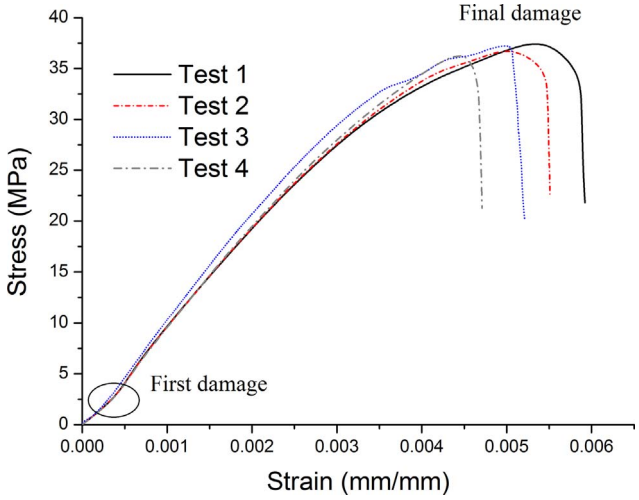

Fig. 7. Typical stress–strain curves for $[90]_4$ laminates.

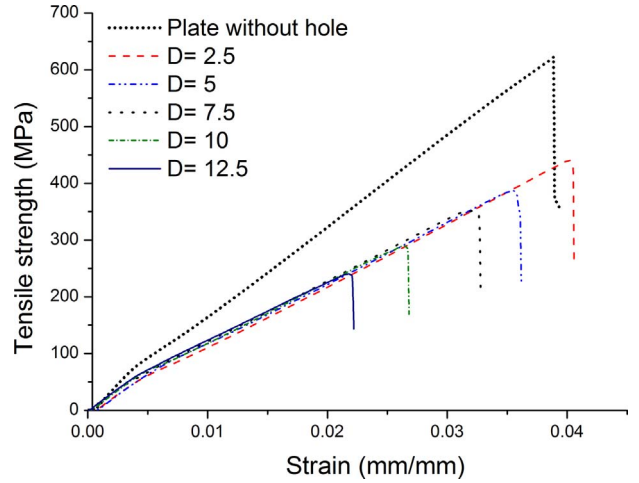

Fig. 8. Comparison of the stress–strain curve for unnotched and notched specimens with various hole diameters.

and pulling-out of fibers that take place in the vicinity of the hole.

Remark: As mentioned earlier, for each shape family, the stress–strain curves have identical behavior and the curves almost overlap each other. This is because that the recorded strain is the far field one. So, the strain will not affect much by the notch size and the recorded strain values will not change relatively during the loading process. For this reason, DIC investigation will be carried out to calculate the strain field around the notch and also to determine the notch size effect on the strain distribution.

Fig. 11 compares the strength degradation of specimens with various fiber orientation angle of perforated composite plates with open hole diameter equal to 4 mm. This notch diameter was chosen to limit the hole size effect and the plate can be considered as infinite. As shown in Fig. 11, the strength degradation was lowest for $[45]_4$, and the strength degradation of $[90]_4$ was smaller than that of $[0]_4$. In these tests, the reason that the $[0]_4$ specimen exhibited more strength degradation during tensile loading than other fiber orientation angle is probably associated with the stress concentration effect. As the fibers are the major load carrying constituents, in $[0]_4$ specimen more fibers are cut that carry the load. Therefore, it results a significant strength degradation. A similar justification can be given for $[45]_4$ and $[90]_4$ specimens. For a better understanding of the strength degradation, an in-depth study on strain and stress distributions will be given in the next section.

Fig. 12 summarizes the experimental data for composite laminate with circular notches for comparison with aluminum specimens. It can be seen from this figure that the degradation of strength was strongly related to the material properties and the size of the open hole. It turned out that as the open hole diameters increased from 2.5 to 12.5 mm, the strength ratio steadily decreased from 0.753 to 0.361 and from 0.521 to 0.314 for laminate and aluminum plates, respectively. The strength degradation of composite material was smaller than that aluminum. More details on the strength behavior using the analytical models will be given in the Section 7 for both composite and aluminum materials. On the other hand, Fig. 13 shows comparison of the tensile strength ratio for the laminated plates with different shape and notch sizes. The strength ratios for plates with rectangular notches are greater than those for square notches.

6.3. Open hole stress distribution

As discussed earlier, the DIC technique was used to obtain the strain fields developed in aluminum plates, composite specimens with various fiber orientation angles (0°, 90° and ± 45°) as well as in specimens with different notch sizes loaded in tension at a rate of 0.5 mm/min. It is shown in Section 4.2 that the technique provides quantitative information that can be used to identify the stress distribution and possible damage zones. A speckle pattern was applied manually on the specimen surface. As the quality of the speckle pattern affects the strain distribution it needs to be carefully dropped. The correlation subset size was large enough to ensure that there was a sufficiently distinctive pattern contained in the area used for correlation. In order to calculate the SCF around the zone of discontinuities, the stress–strain relationship was used for planar composite structures. Four fiber orientation angles are chosen to validate the FE models with the experimental and approximate analytical solution. DIC technique measurements were carried out in all the samples. The SCF results tabulated in Table 2, are actually the average of three values obtained for each specimen. It can be seen that the FE outputs are in good agreement with both approximate analytical and experimental results, and the difference between them is considered insignificant. However, an important difference can be noted comparing experimental findings with FEM and analytical solution for composite laminate when $\theta = 90°$. So, it is important to realize that the experimental measurements consider the real deformation of the composite specimens, and it is very difficult to generate a suitable pattern for all the specimens with manual paint. On the other hand, it can be concluded that the stress concentration phenomena explain the strength degradation in specimens with different fiber orientation angle. It turned out that the strength load decreases as the stress concentration increases.

The validity of Eq. 2, multiplied by the correction factor K_T/K_T^{∞}, is

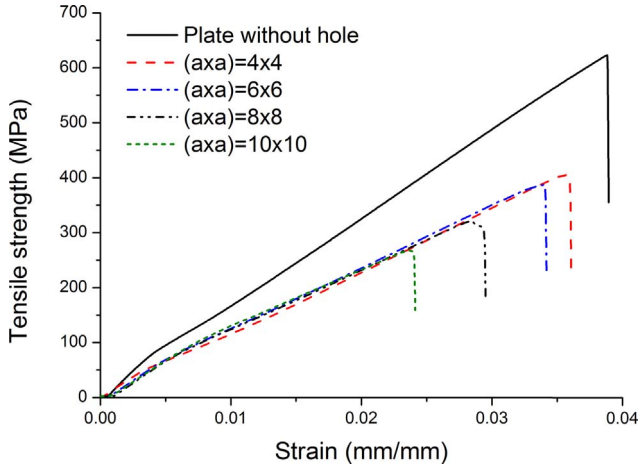

Fig. 9. Comparison of the stress–strain curve for unnotched and notched specimens with various square holes.

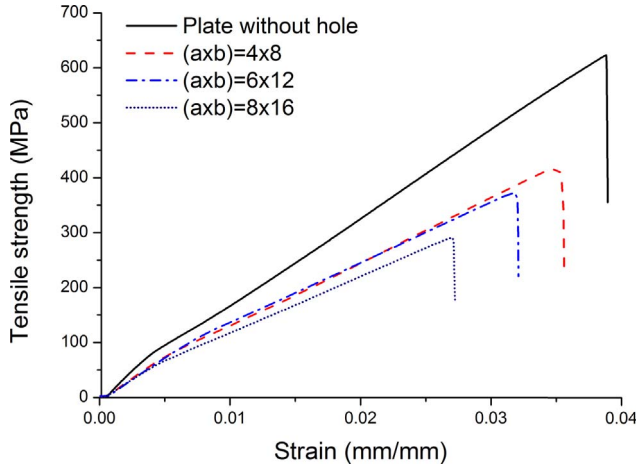

Fig. 10. Comparison of the stress–strain curve for unnotched and notched specimens with various rectangular hole.

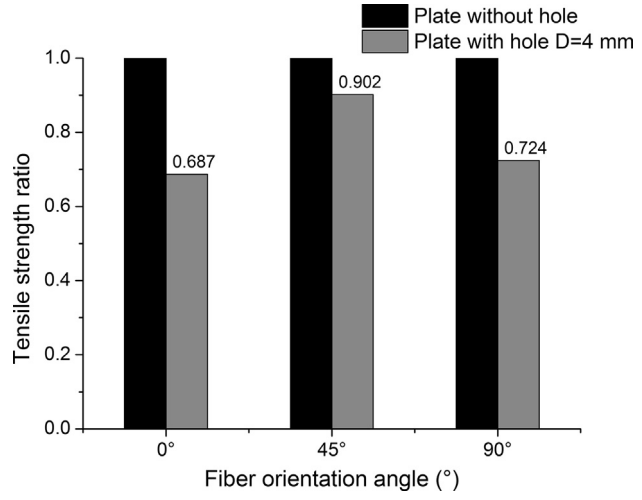

Fig. 11. Comparison of the tensile strength for unnotched and notched specimens with various fiber orientations.

verified in Figs. 15 and 14 by comparing the stress distribution obtained analytically with the FEA results of the notched laminates as well as aluminum specimens with different circular notch sizes under tensile load.

It can be seen from the figures that for both materials, with the increase of the circular notch diameter, the stress increases in a non-linear manner. Moreover, at and near the hole edge, the analytical results are very close to the FEM, and further away from the hole, the analytical results differ very much from the FEM except for plates with a hole diameter less than or equal to 5 mm, which simulates the results of a hole in an infinite width plate. It should be noted that the approximate analytical solution multiplied by the correction factor may not be accurate enough for large notch size (more than 5 mm in our study, $D/W = 0.2$), for comparisons with FE calculations that give accurate stresses at nodal points.

In addition to the stress curves given for circular holes, laminated plates with no-circular notches are analyzed to study the influence of the hole shape effect on the stress distributions. There are two sets of numerical results, one for square notches and the second for rectangular

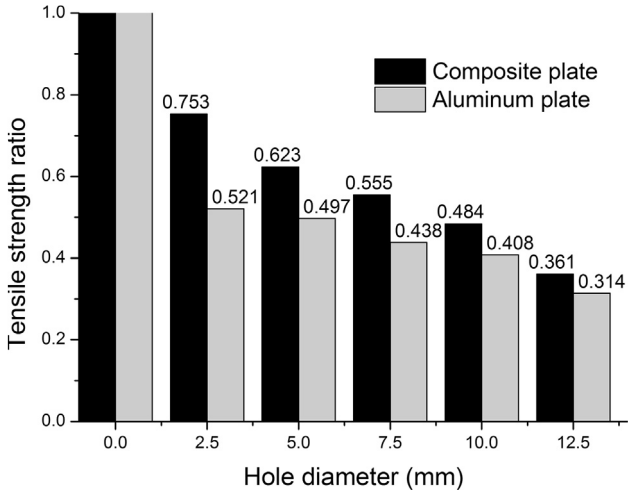

Fig. 12. Comparison of the tensile strength ratio for composite and aluminum unnotched and notched specimens with various hole diameter.

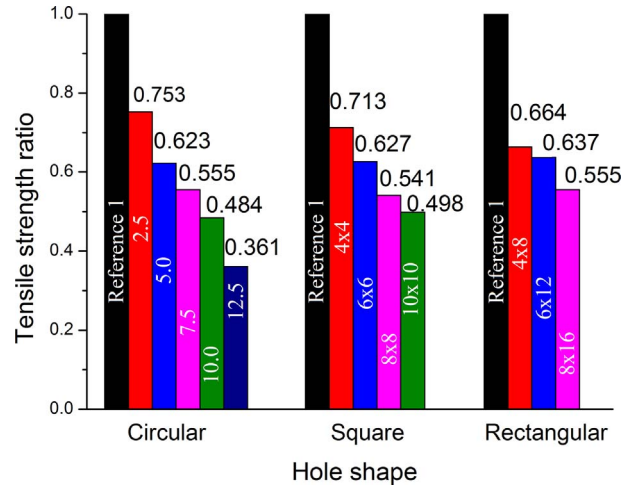

Fig. 13. Comparison of the tensile strength ratio for composite unnotched and notched specimens with different shape holes.

Table 2
SCF for plates with different fiber orientation angles under tensile load.

Materials	Fiber Orientation	Analytical	FEM	Experimental
Aluminum	–	3.000	3.117	3.695
E-Glass/Epoxy	0°	3.939	4.047	4.224
	45°	2.827	2.776	3.184
	−45°	2.827	2.776	3.358
	90°	3.047	3.151	1.655

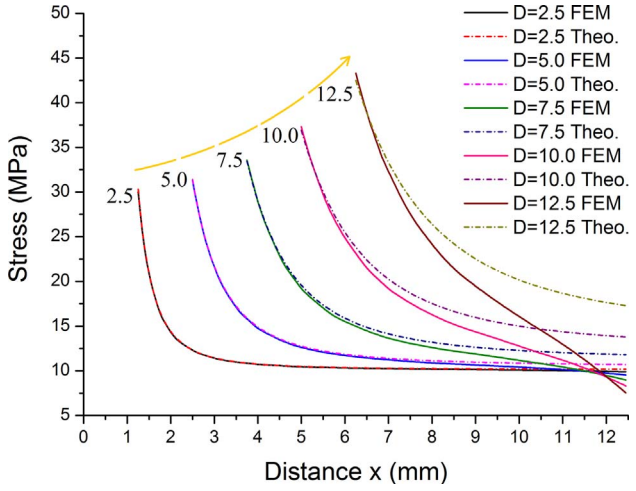

Fig. 14. Comparison of the analytical/FEM stress distributions for aluminum specimens with various hole diameters.

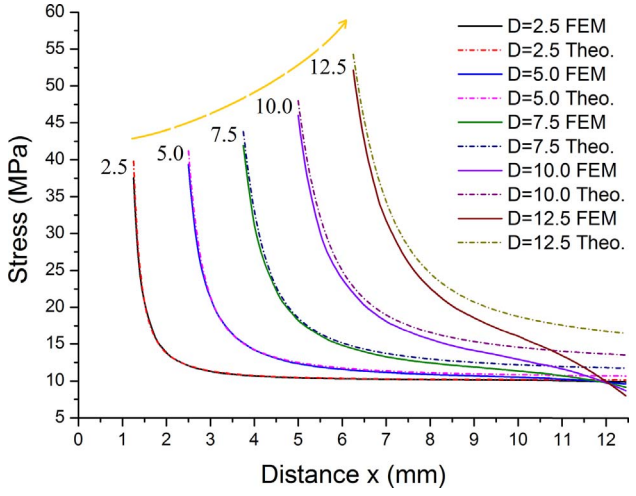

Fig. 15. Comparison of the analytical/FEM stress distributions for laminated specimens with various hole diameters.

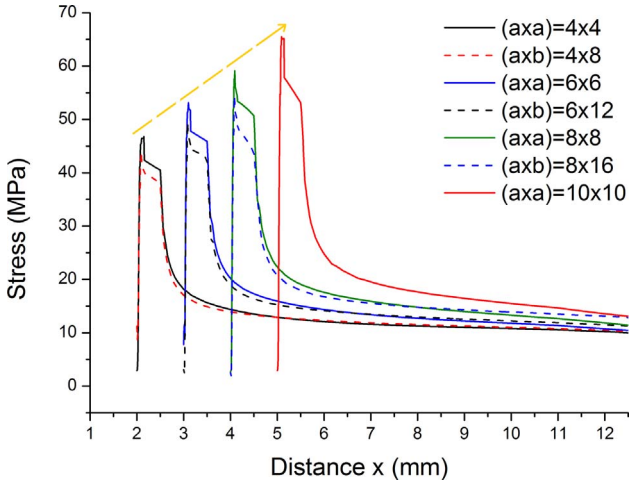

Fig. 16. FEM stress distributions for laminated specimens with rectangle and square notches.

holes. The results are plotted by solid and dashed lines in Fig. 16, respectively. FE stresses on and near the notch boundary and in the far field along *x*-axis are plotted for specimens with various notch sizes. From the Fig. 16, it is clearly seen that with the increase of the notch

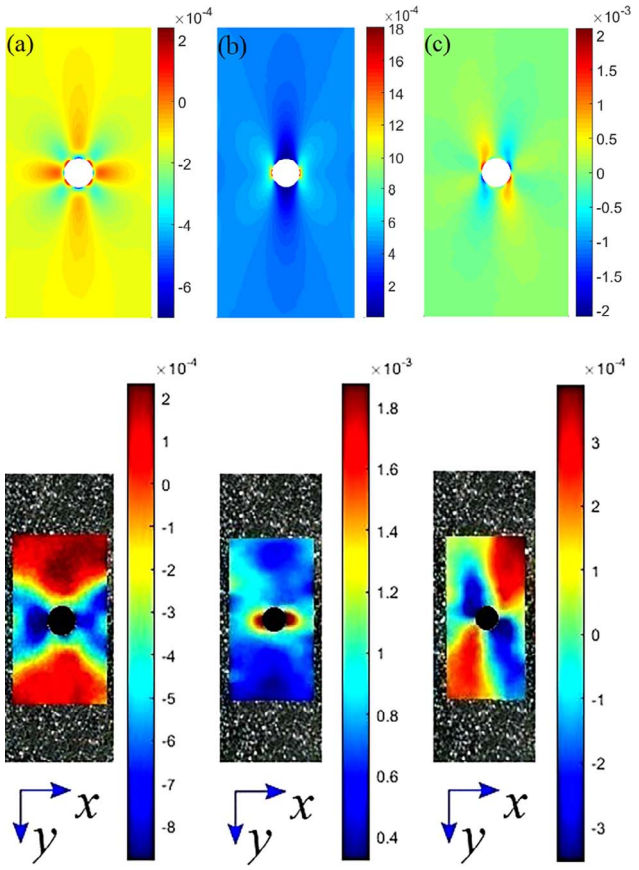

Fig. 17. FEA and DIC engineering strain fields for $[0]_4$ notched laminate (D = 5 mm); (a) ϵ_{xx}, (b) ϵ_{yy} and (c) ϵ_{xy} distributions.

size, the stress increases in a linear manner. Laminated plates with rectangular notches have lower stress compared to square notches. This means that the increase of the square hole side, parallel to the applied load, will lead to the minimization of maximum stress by smoothing the stress distribution. Moreover, the stress is relatively equal to 0 on the left side of the right top corner. Then it can be seen the stress jumping from 0 to a maximum value. Further, away from the notch corner, the stress is slightly reduced till it reaches the applied load far away from the hole.

6.4. Open hole DIC strain fields

6.4.1. Strain distributions around circular holes

The strain fields obtained by the DIC technique as well as the final catastrophic failure observed for different open notch size are shown in Figs. 17–22. In order to validate the DIC measurements, the experimental strain distribution have been compared to the FE output results. Fig. 17–22 show the three in-plane strain fields (ϵ_{yy} (load direction), ϵ_{xx} (transverse direction) and ϵ_{xy}) in the cutout region obtained by DIC and FEA output under elastic applied load. The results show very high localized strains at the opening boundary. The strain concentration zone increases as the notch size increases. This phenomenon explains the increase of the SCF and the damage zone observed in the previous section.

Figs. 17 and 18 show the DIC and FEA results in terms of engineering strain plots ϵ_{xx},ϵ_{yy} and ϵ_{xy} for laminate plate with open notch diameters equal to 5 and 7.5 mm, respectively. As shown in these figures, the ϵ_{yy} strain is concentrated on two points located at ± 90° respecting the load direction ($\epsilon_{yy} = 1.91 \times 10^{-3}$ for D = 7.5 mm) and fiber breakage would be expected at this strain level, which is not captured by DIC technique. The ϵ_{xy} strain distribution although relatively low, in

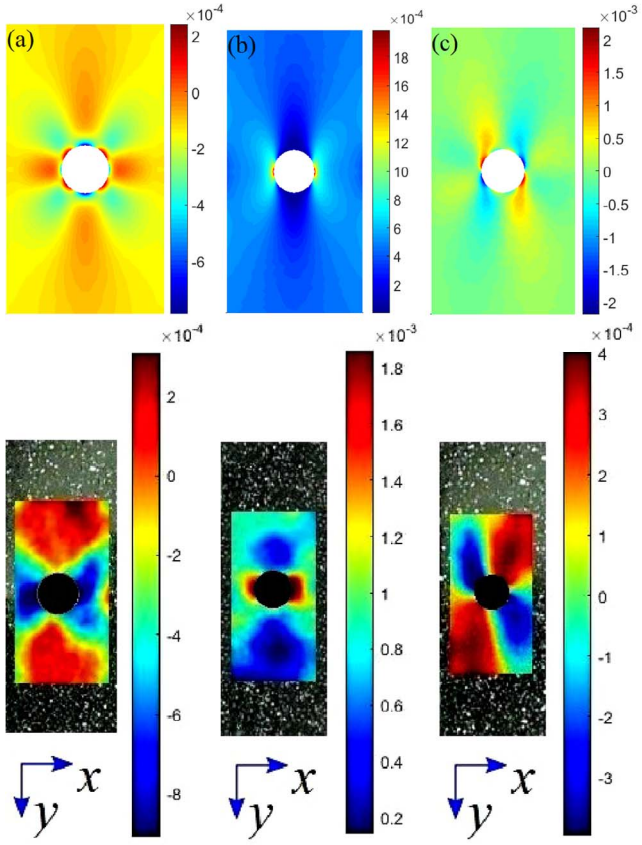

Fig. 18. FEA and DIC engineering strain fields for $[0]_4$ notched laminate (D = 7.5 mm); (a) ϵ_{xx}, (b) ϵ_{yy} and (c) ϵ_{xy} distributions.

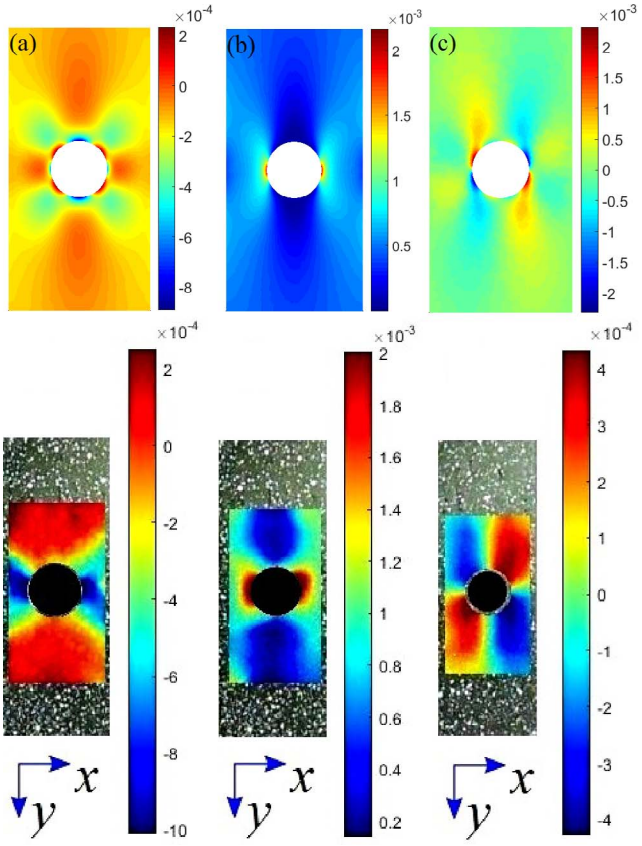

Fig. 20. FEA and DIC engineering strain fields for $[0]_4$ notched laminate (D = 10 mm); (a) ϵ_{xx}, (b) ϵ_{yy} and (c) ϵ_{xy} distributions.

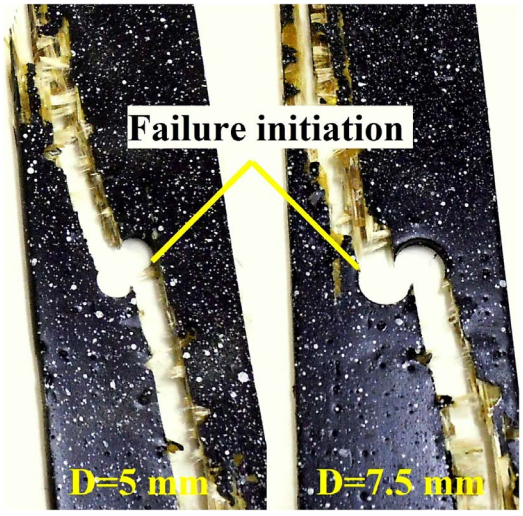

Fig. 19. Final failure of a $[0]_4$ laminate notched specimens (D = 5 and 7.5 mm).

combination with high longitudinal strain ϵ_{yy}, introduces damage in the form of longitudinal splitting as shown in the final failure picture of Fig. 19.

Fig. 19 shows a typical local view of region around the notches and describes the main damage of laminated specimens, showing cracks, fiber breakages and splitting bounds. All these damages initiated firstly from the notch edge. The main damage mechanism observed in the laminates was first initiation of damage at ± 90° respecting the load direction. Then the damage mechanism was splitting at the cutout boundary along the fibers direction and parallel to the loading axis. Fig. 19 shows the final catastrophic failure of a $[0]_4$ notched specimen with holes of D = 5 and 7.5 mm. For laminated specimens with hole diameter less than 7.5 mm, the open hole has completely been isolated by 0° splits respecting the load direction and the specimen behaves like the one with no hole. The damage here acts as a 'crack stopper' leading to a notch insensitive behavior of the composite laminate. This observation is consistent with the results given in [2].

Figs. 20 and 21 depict the DIC and the FEA results in terms of engineering strain plots for open notch laminate with opening diameter equal to 10 and 12.5 mm, respectively. The longitudinal strain values increase as the notch size increase and the maximum value of ϵ_{yy} estimated by the DIC is approximately 2.1×10^{-3} for D = 12.5 mm. For plates with large open notch diameters, both fiber breakage and fiber–matrix interface failure are expected to occur at this strain level. The results show very high localized ϵ_{yy} strain near the hole, concentrated on two points located at ± 90° respecting the load direction and creating the first damage locations.

In Fig. 22, the behavior of the D = 10 and 12.5 mm notched specimens is presented. The final failure occurs at an applied stress of 274.86 and 204.59 MPa, respectively. In this case also, damage initiated firstly from the notches edges and high normal strain generated here. For specimens with open hole diameter greater than 7.5 mm, the main damage mechanism observed in the specimens was a first initiation of damage at ± 90°. As loading increased, these small damage regions started to propagate along fiber direction. When growing big enough, the damage zone around the notch region will be extensive. The failure mechanism was mixed between transverse cracking and splitting at the cutout boundary along the transverse-longitudinal directions, respectively. Other specimens have a fracture surface almost perpendicular to the loading axis. This failure mechanism can be explained by the edge effect and the high localized strain/stress concentration. This causes 90° transverse cracks near the hole region while the shear strain ϵ_{xy} drive axial splits, parallel to the loading axis.

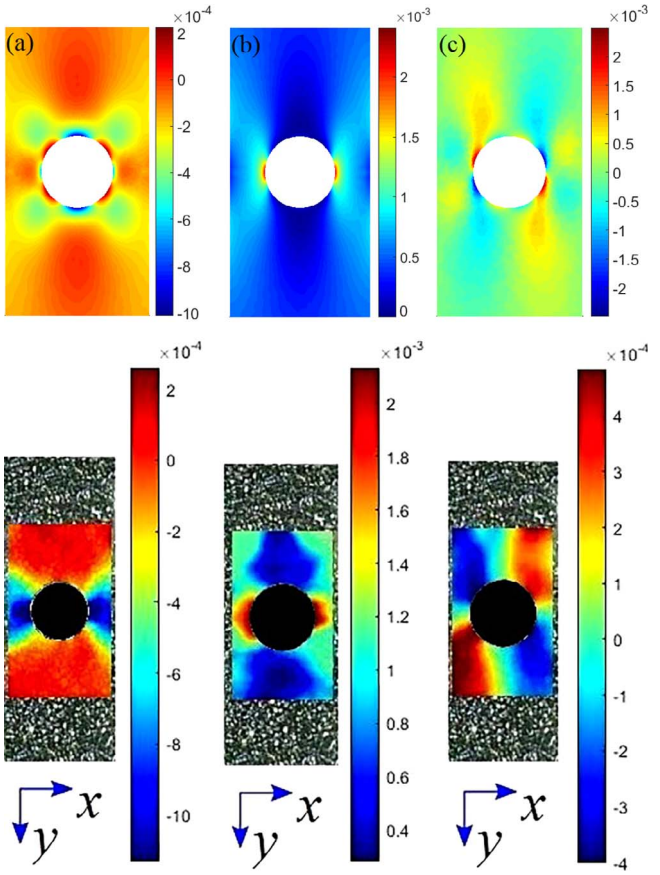

Fig. 21. FEA and DIC engineering strain fields for $[0]_4$ notched laminate (D = 12.5 mm); (a) ϵ_{xx}, (b) ϵ_{yy} and (c) ϵ_{xy} distributions.

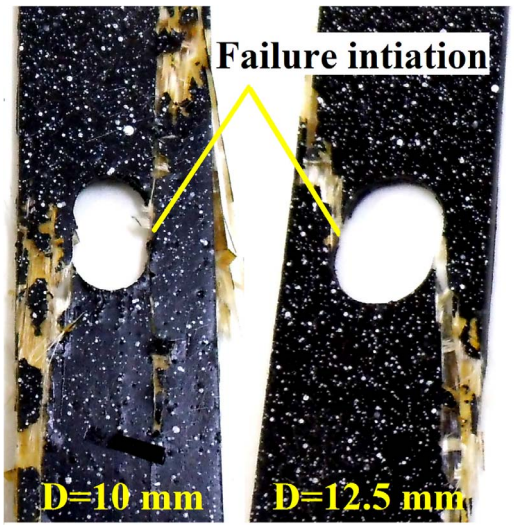

Fig. 22. Final failure of a $[0]_4$ laminate notched specimens (D = 10 and 12.5 mm).

6.4.2. Strain distributions around square and rectangular holes

To clarify the effect of square and rectangular notch sizes on the strain distribution and failure mechanism, it is again useful to use the DIC technique in this investigation. Strain distributions at and near the notch boundary and in the far field along the horizontal and vertical axes are given in Fig. 23–28. In this case also, the experimental strain distributions have been compared to the FE output results to validate the DIC measurements. $[0]_4$ plates with rounded square and rectangular holes were subjected to far-field load and the strain concentration at the corners is of interest. It is noted that in this kind of notches, one can

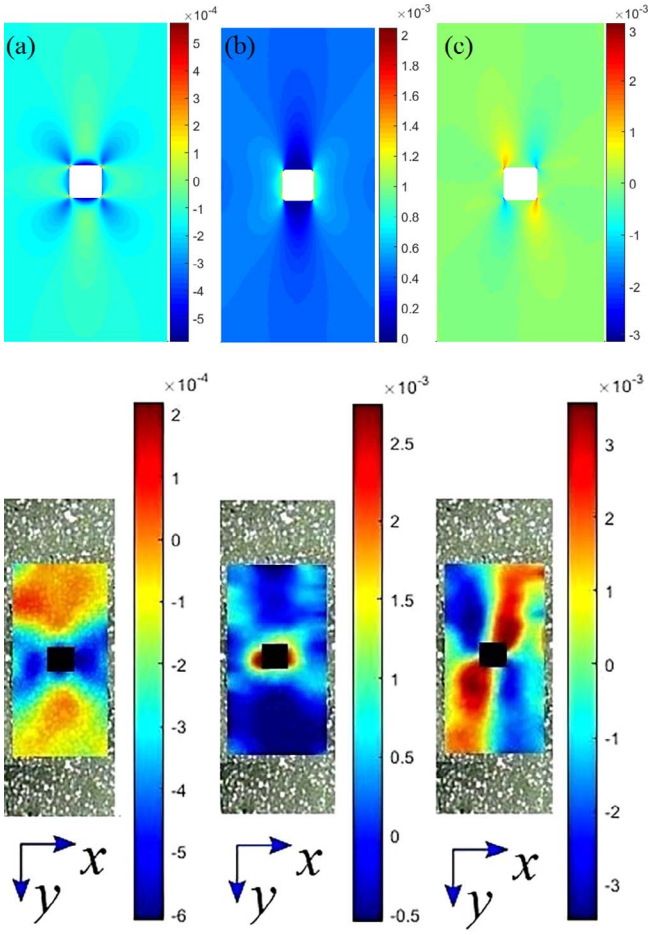

Fig. 23. FEA and DIC engineering strain fields for $[0]_4$ notched laminate ($4 \times 4\ mm^2$); (a) ϵ_{xx}, (b) ϵ_{yy} and (c) ϵ_{xy} distributions.

focus only on the strain concentration at the corner of the hole, because these corners are the locations of cracks and fracture initiations. The above mentioned figures show the three in-plane strain fields (ϵ_{yy},ϵ_{xx} and ϵ_{xy}) in the cutout region obtained by DIC and FEA outputs. Once these strains are calculated, the stress–strain relationship for planar composite structures is used to find the stress concentration. In the following, the accuracy and applicability of the DIC technique and FE models are examined through a series of examples. The first two examples are plates with square holes of 4×4 and $6 \times 6\ mm^2$ sizes with rounded corners.

It can be seen that the FE models can produce good results for the strain or stress concentration. The results show very high localized strains at the notch corners. The strain field is dominated by the strain patterns associated with the nearby corner, and the strain patterns from neighboring corners are of negligible magnitudes. On the other hand, the strain concentration zone increases as the notch size increase. Furthermore, as shown in these figures, the ϵ_{yy} strain is concentrated on the four corners (2.3×10^{-3}) for $(a \times a = 6 \times 6\ mm^2)$ and fiber breakage would be expected at this strain level. The ϵ_{xy} strain distribution although relatively low, in combination with high longitudinal strain ϵ_{yy}, introduces damage in the form of longitudinal splitting as shown in the final failure picture (see Fig. 25).

Fig. 25 shows a typical local view of region around the square notches and describes the main damage of laminated specimens, showing fiber breakages and splitting bounds. The main damage mechanism observed in laminates with 4×4 and $6 \times 6\ mm^2$ square notches was a first initiation of damage at two opposite corners. As the loading increased, the damage was splitting at the cutout boundary along the fibers direction parallel to the loading axis. Fig. 25 shows the

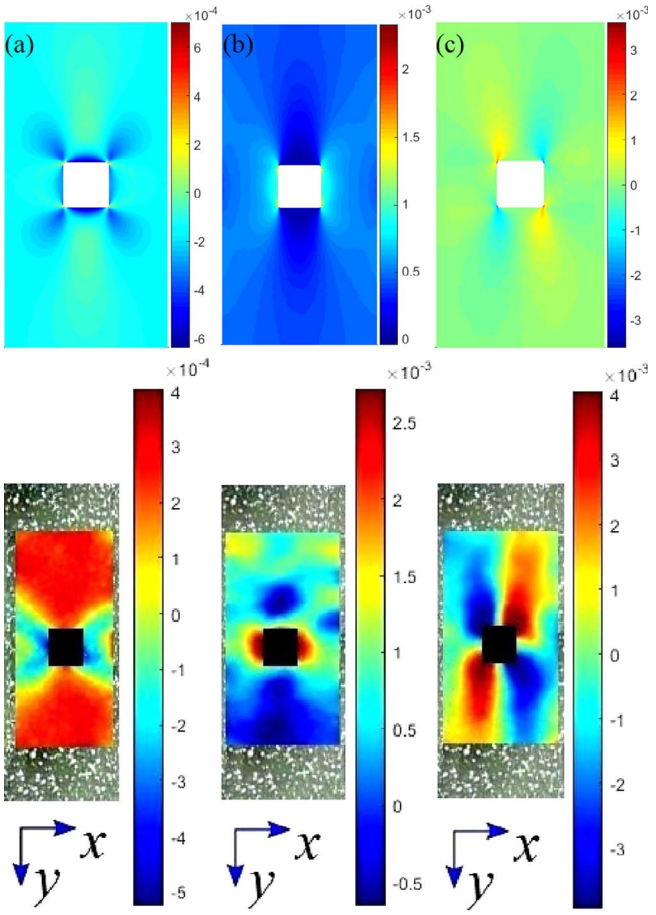

Fig. 24. FEA and DIC engineering strain fields for $[0]_4$ notched laminate ($6 \times 6\,mm^2$); (a) ϵ_{xx}, (b) ϵ_{yy} and (c) ϵ_{xy} distributions.

Fig. 25. Final failure of a $[0]_4$ laminate notched specimens ($a \times a = 4 \times 4$ and $a \times a = 6 \times 6\,mm^2$).

final failure mode of a $[0]_4$ notched specimen. The end result is that for laminated specimens with square hole length less than 6 mm, the square notch has completely been isolated by 0° splits respecting the load direction.

The second examples are similar to the first except that the square

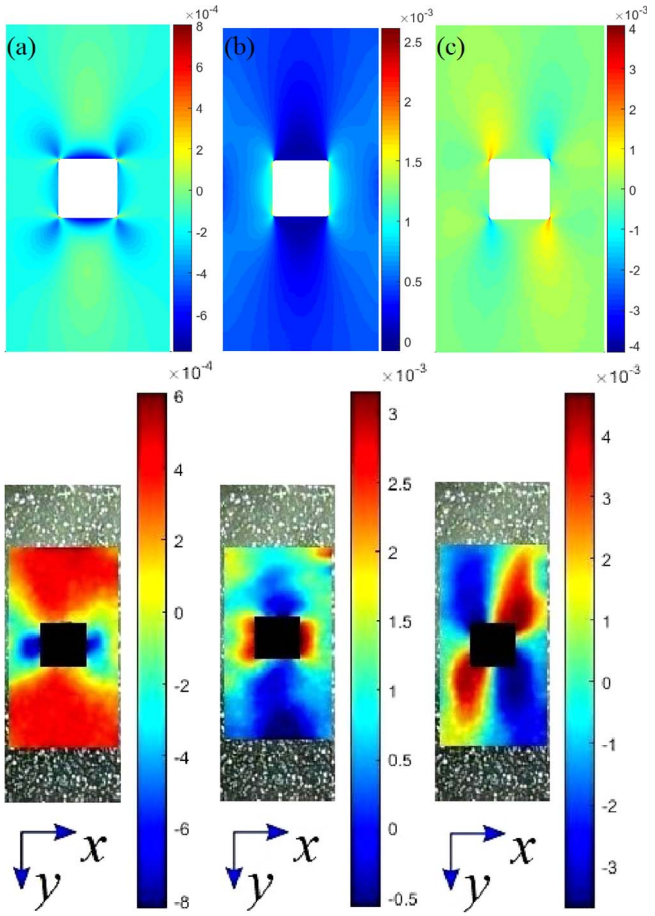

Fig. 26. FEA and DIC engineering strain fields for $[0]_4$ notched laminate ($8 \times 8\,mm^2$); (a) ϵ_{xx}, (b) ϵ_{yy} and (c) ϵ_{xy} distributions.

notch lengths are $a \times a = 8 \times 8$ and $10 \times 10\,mm^2$. The engineering strain distributions obtained using the DIC experiments and the FEM are plotted in Figs. 26 and 27. The comparison of the obtained results is very similar to the comparison given for the Figs. 23 and 24. The main difference is that for larger square holes, the fracture path is different compared to the first cases, as we will discuss in the following. This is because of the edge notch effect. Moreover, the longitudinal strain values increase as the notch size increases and the maximum value of ϵ_{yy} estimated by the FEM is approximately 2.8×10^{-3} for $10 \times 10\ mm^2$ square hole. For plates with large square notch, both fiber breakage and fiber–matrix interface failure are expected to occur at this strain level. The results show very high localized ϵ_{yy} strain concentrated on four points located at the corners creating the first damage locations as shown in Fig. 28.

In Fig. 28, the fracture behavior of the $a \times a = 8 \times 8$ and $10 \times 10\,mm^2$ notched specimens is presented. The final failure occurs at an applied stress of 307.32 and 282.83 MPa, respectively. For specimens with square hole length greater than 6 mm, the main damage mechanism observed in the specimens was a first initiation of damage at two opposite corners. As loading increased, these small damage regions tried to propagate along fiber direction. When growing big enough, they became the splitting bands towards the free edge. Extensive damage area around the free edge on the cross line of the notch generated delaminations along fiber direction ($a \times a = 10 \times 10\,mm^2$). The final failure mechanism was mixed with transverse cracking and splitting at the cutout boundary along the transverse-longitudinal directions, respectively. Other specimens have a fracture surface almost perpendicular to the loading axis. The final failure mechanism can be explained by the edge effect, fiber breakages happened in some weak

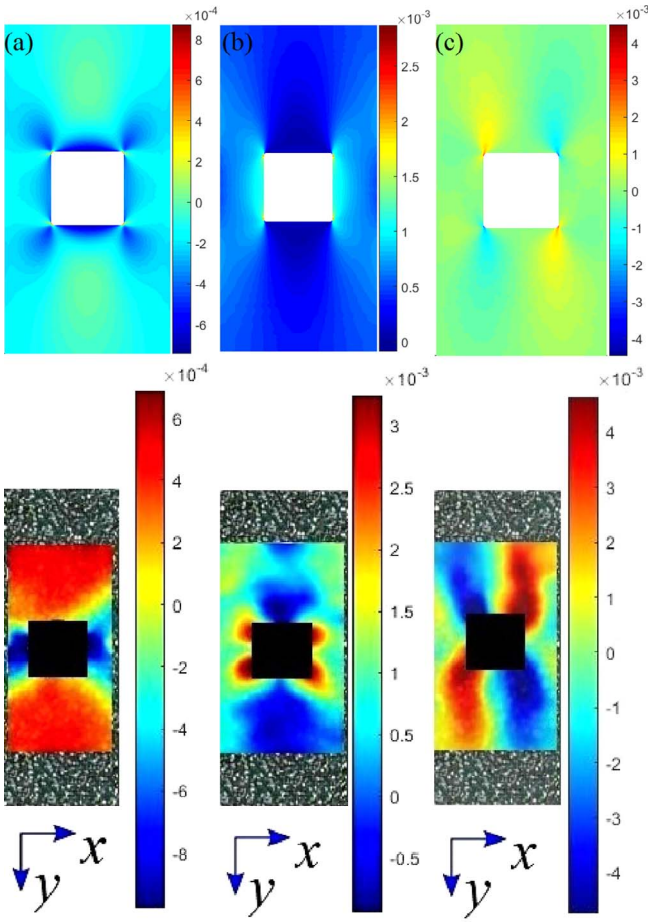

Fig. 27. FEA and DIC engineering strain fields for $[0]_4$ notched laminate ($10 \times 10\,mm^2$); (a) ϵ_{xx}, (b) ϵ_{yy} and (c) ϵ_{xy} distributions.

Fig. 28. Final failure of a $[0]_4$ laminate notched specimens ($a \times a = 8 \times 8$ and $a \times a = 10 \times 10\,mm^2$).

regions and the high localized strain–stress concentration causes transverse cracks near the hole region while the shear strain ϵ_{xy} drive delamination and axial splits, parallel to the loading axis.

For the next three examples, laminated plate with rectangular

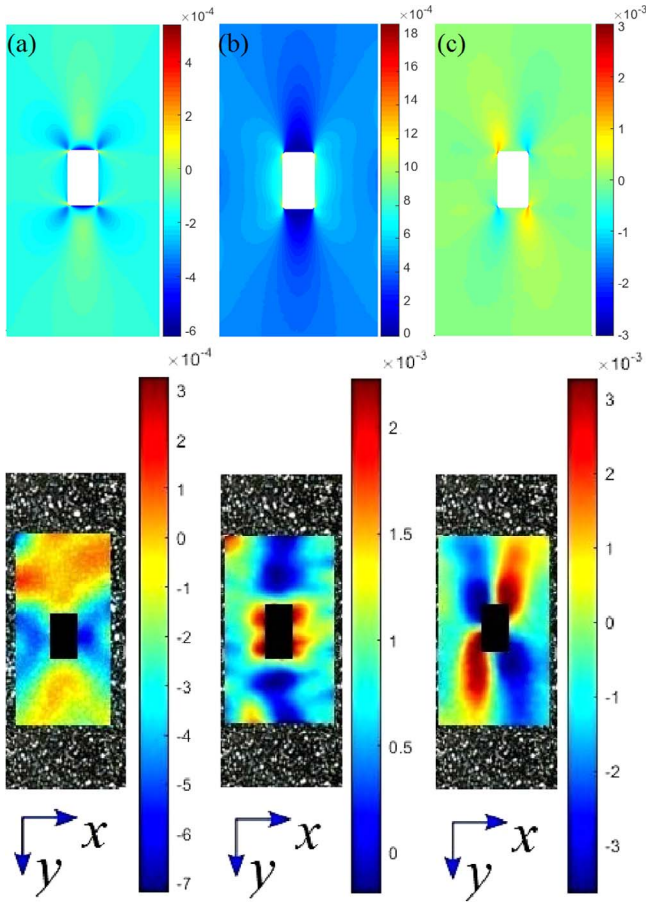

Fig. 29. FEA and DIC engineering strain fields for $[0]_4$ notched laminate ($4 \times 8\,mm^2$); (a) ϵ_{xx}, (b) ϵ_{yy} and (c) ϵ_{xy} distributions.

openings with rounded corners shown in Figs. 29–31 are analyzed. The strain distributions are plotted in the same manner as in the preceding cases. The results for these cases are similar to those obtained for square notches. Again it can be seen that the FEM can provide good results for these examples. Moreover, the strain concentration in these cases are less compared to those obtained for square notches with the same lower length and radii curvature. This means that the increase of the square hole side, parallel to the applied load, will lead to the minimization of maximum strain by smoothing the strain distribution. In these cases again, the fracture locations (see Fig. 32) are clearly seen at the corners of the rectangular notches. The final failure loads are 377.16, 361.66 and 315.26 MPa for $a \times b = 4 \times 8{,}6 \times 12$ and $8 \times 16\,mm^2$, respectively.

The SCF obtained using FEM and DIC are summarized in Table 3. Compared to experimental data, the accuracy of the numerical results is within 18%. The DIC technique remains more practical in these kind of problems (notch with corners), because the strain analysis of plates with square and rectangular notches with small radii of curvature is far more computationally challenging than cases where the radii are large. At very small radii of curvature, the FEA would be unable to produce very accurate strain–stress results at the notch corners. To obtain very accurate strain results at such small radii, adaptive fine meshes are needed in the FEA. However, The FEM remains practical because compared to experimental findings the accuracy of the obtained results are within 18%.

7. Experimental and analytical open hole tensile strength

The characteristic length d_0 is estimated from Eq. 4 using the experimental tensile strengths of the unnotched and notched specimens,

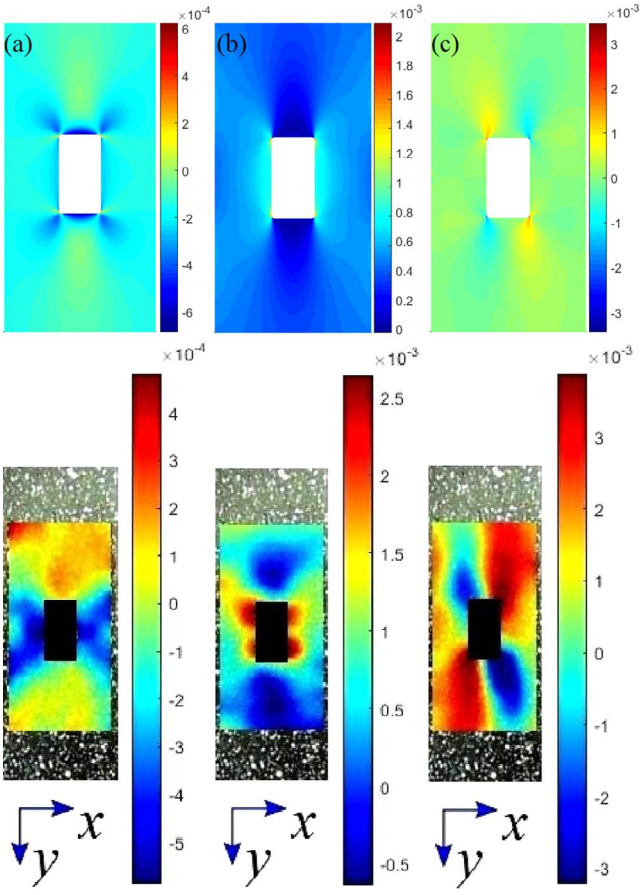

Fig. 30. FEA and DIC engineering strain fields for $[0]_4$ notched laminate ($6 \times 12\,mm^2$); (a) ϵ_{xx}, (b) ϵ_{yy} and (c) ϵ_{xy} distributions.

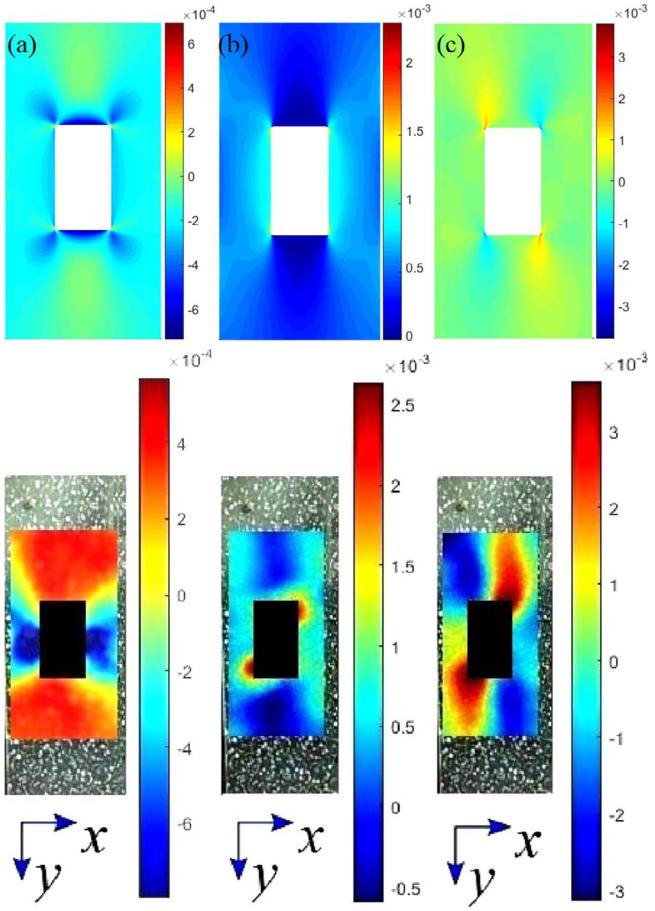

Fig. 31. FEA and DIC engineering strain fields for $[0]_4$ notched laminate ($8 \times 16\,mm^2$); (a) ϵ_{xx}, (b) ϵ_{yy} and (c) ϵ_{xy} distributions.

the width of the specimens and the notch radius. As discussed earlier, the notched strength σ_{Nh}^{∞} is obtained from the experimental notched strength multiplied by the correction factor K_T/K_T^{∞}. The characteristic length, for both composite and aluminum materials, can be obtained from Eq. 4 using the Newton–Raphson iterative scheme [43]. Table 4 and 5 present the SCF obtained by the analytical solution, FEA output and the DIC technique as well as the tensile strength of notched specimens and the characteristic length. It can be seen from these results that the SCF and the characteristic length increases and the notched strength decreases with increase in the notch diameter. The increase in strain concentration and damage zone observed in the final failure pictures explain clearly the increase in characteristic length. Comparison of experimental data [17,21,44–47] has also shown that characteristic lengths are material and hole size dependent [22]. This calls for using the modification of point stress criterion models proposed by Kim et al. [21] and Kannan et al. [22] to predict the notched tensile strength. In Kim et al. [21] and Kannan et al. [22] models, the tensile fracture parameters (k,m) and (k_f,m_f) in Eqs. 5 and 6 are to be determined using the experimental data for both equations, $d_0 = f(2R/W)$ and $\sigma_0\sqrt{\pi d_0}/k_f = f(\sigma_{Nh}^{\infty}/\sigma_0)$, respectively. These parameters are to be determined by least square curves fit to the data (see Fig. 33–36). Two notched specimen tests in addition to an un-notched specimen test are required. In this experimental investigation, more tests are performed to take into account the scatter in test results.

The values of the fracture parameters calculated form the experimental results, for both aluminum and composite materials, are summarized in Table 6. Now, the tensile strengths σ_{Nh} using Kim's model can be predicted using the following equation

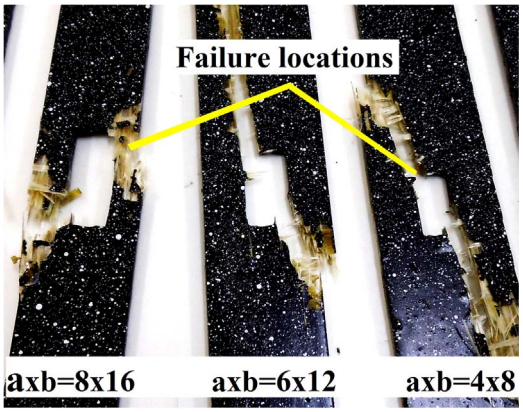

Fig. 32. Final failure of a $[0]_4$ laminate notched specimens ($a \times b = 4 \times 8{,}6 \times 12$ and $8 \times 16\,mm^2$).

Table 3
Experimental and numerical SCF for composite material with different shape notches.

Circular notch			Square notch			Rectangular notch		
D (mm)	FEM	DIC	$a \times a$ (mm^2)	FEM	DIC	$a \times b$ (mm^2)	FEM	DIC
2.5	3.756	4.114	4 × 4	4.682	5.721	4 × 8	4.399	5.212
5	3.937	4.025	6 × 6	5.313	5.956	6 × 12	4.946	5.676
7.5	4.194	4.799	8 × 8	5.917	7.032	8 × 16	5.442	6.086
10	4.601	5.072	10 × 10	6.551	7.229	–	–	–
12.5	5.213	5.122	–	–	–	–	–	–

Table 4
SCF and notch strength results for composite material.

$2R/W$	SCF			Fracture strength			Charac. length d_0 (mm)
	Analytical solution	FEM	Test	σ_{Nh} (MPa)	σ_{Nh}^{∞} (MPa)	$\sigma_{Nh}^{\infty}/\sigma_0$	
0.1	3.981	3.756	4.114	427.570	432.151	0.761	0.847
0.2	4.122	3.937	4.025	353.541	369.928	0.652	1.039
0.3	4.384	4.194	4.799	314.932	350.540	0.618	1.347
0.4	4.801	4.601	5.072	274.861	334.991	0.590	1.595
0.5	5.428	5.213	5.122	204.590	281.960	0.497	1.304

Table 5
SCF and notch strength results for aluminum material.

$2R/W$	SCF			Fracture strength			Charac. length d_0 (mm)
	Analytical solution	FEM	Test	σ_{Nh} (MPa)	σ_{Nh}^{∞} (MPa)	$\sigma_{Nh}^{\infty}/\sigma_0$	
0.1	3.023	3.004	3.272	83.751	84.648	0.527	0.330
0.2	3.140	3.131	3.648	79.850	83.578	0.520	0.633
0.3	3.347	3.358	3.716	70.380	78.523	0.489	0.778
0.4	3.693	3.732	4.338	65.572	80.722	0.502	1.139
0.5	4.250	4.330	4.766	50.401	71.399	0.444	0.901

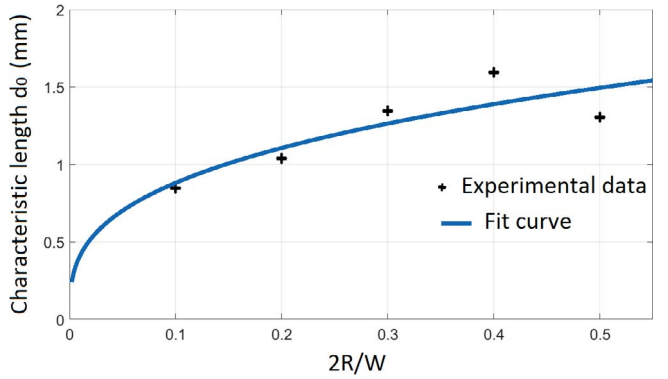

Fig. 33. Values of characteristic length according to $2R/W$ for laminate specimens.

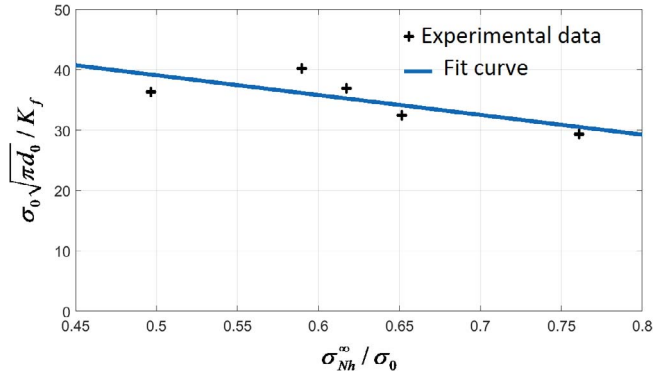

Fig. 34. The critical stress intensity factor according to the strength ratio for laminate specimens.

$$\sigma_{Nh}^{\infty}/\sigma_0 = \frac{2}{2 + A_0^2 + 3A_0^4 - (k_T^{\infty} - 3)\{5A_0^6 - 7A_0^8\}}, A_0 = \frac{1}{1 + 2^m R^{m-1} W^{-m} K^{-1}} \tag{23}$$

On the other hand, the tensile strength is obtained based on Kannan's model by using Eq. 6 in Eq. 5 for eliminating the characteristic length d_0. The nonlinear fracture strength equations are solved using the Newton–Raphson iterative method to obtain the notched strength

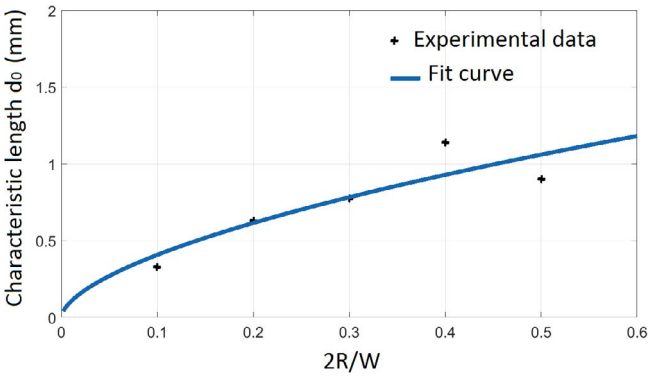

Fig. 35. Values of characteristic length according to $2R/W$ for aluminum specimens.

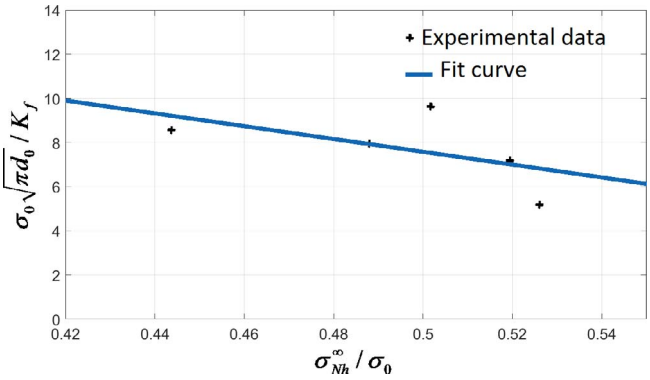

Fig. 36. The critical stress intensity factor according to the strength ratio for aluminum specimens.

Table 6
Tensile fracture parameters for composite and aluminum materials.

Materials	Fracture parameters				
	σ_0 (MPa)	k	m	k_f (MPa$\sqrt{m}$)	m_f
Aluminum	160.91	0.557	0.703	22.081	1.314
E-Glass/Epoxy	576.92	0.522	0.319	55.499	0.592

Table 7
Comparison of notched tensile strength estimates with test data for laminate specimens.

$2R/W$	SCF	Fracture strength σ_{Nh} (MPa)				
		Test	Model 1	Relative error in %	Model 2	Relative error in %
0.1	3.981	427.571	429.003	0.336	434.186	1.548
0.2	4.122	353.540	359.838	1.782	362.284	2.474
0.3	4.384	314.930	306.807	−2.578	307.073	−2.494
0.4	4.801	274.862	260.171	−5.345	258.684	−5.886
0.5	5.428	204.591	216.881	6.008	214.176	4.686

σ_{Nh}^{∞} of the infinite plate for the specified notch size. The notched strength σ_{Nh} of the finite width specimen is then obtained by dividing σ_{Nh}^{∞} with the correction factor. Table 7 and 8 give the notched tensile strength of open hole composite and aluminum plates from the modified point stress models. The notched tensile strength estimates, by both models, are found to be within 17% of test results.

Remark: As mentioned in Kannan et al. [22], whenever m_f is found to be greater than unity, the parameter m_f has to be truncated to 1 by suitably modifying the parameter k_f with the fracture data. In our study, the aluminum material has $m_f = 1.314$. Based on Kannan et al. [22] remark, the parameter m_f is truncated to 1.0 and the new k_f is equal to 28.989.

Table 8
Comparison of notched tensile strength estimates with test data for aluminum specimens.

		Fracture strength σ_{Nt} (MPa)				
$2R/W$	SCF	Test	Model 1	Relative error in %	Model 2	Relative error in %
0.1	3.023	83.75	85.914	2.584	78.331	6.47
0.2	3.140	79.85	77.612	−2.804	66.773	16.37
0.3	3.347	70.38	70.212	−0.241	62.773	10.80
0.4	3.693	65.57	62.092	−5.306	57.328	12.56
0.5	4.250	50.40	52.984	5.126	50.697	−0.60

8. Conclusion

In the present work, digital image correlation (DIC) technique was used for the assessment of strain–stress distributions and failure mechanisms taking place in aluminum as well as in composite laminates with various notch shapes and sizes loaded in tension. Laminated plates with circular, square and rectangular notches were used in this investigation. In addition, approximate analytical solution and FEM were also used to validate the experimental results and investigate the tensile strength degradation in specimens with different open hole sizes and fiber orientation angles. The DIC technique was successfully applied to determine the surface strains and relate to possible failure mechanisms that could occur in different specimens. The key points that can be concluded from this study are:

- The failure of the specimens was dominated by strain concentration and fiber breakage due to weak notch region and hole edge effect. Strain measurements and SCF, for various circular notch sizes, were compared to approximate analytical solution with a good agreement. The high localized strains identified by the DIC technique were also in agreement with the final observed damage mechanism.
- It has been shown that tensile strength degradation and final damage mechanism that appear after final failure are depending on hole shape, open notch size, fiber orientation angle and stress distribution. It can be seen that the SCF and the damage zone increase and the notched strength decreases with increase in the notch size.
- Moreover, the stress concentration around rectangular notches are less compared to those obtained for square notches with the same lower length and radii curvature (for example, The SCF is equal to 5.721 and 5.212 for $a \times b = 4 \times 8$ and $a \times a = 4 \times 4\,mm^2$, respectively). As a consequence, the ultimate strength loads are greater (7% greater compared to square notch). This means that the increase of the square hole side, parallel to the applied load, will lead to the minimization of maximum strain by smoothing the strain distribution and lead also to the maximization of the ultimate load.
- The fiber breakage and the crack propagation, after final failure, coincide with the high strains developed around the hole region and successfully captured by DIC. Similar success was also achieved in the stress distribution assessment where parametric study models were developed for aluminum and laminated notched specimens under tensile loading and the DIC full-field strain measurements were in good agreement with FE results.
- In the second part of this study, the experimental data was used to verify the capability of two modified stress criteria models for predicting tensile strength. It is shown that the modified models are able to predict tensile strengths of notched samples that display different strain gradients. Compared to experimental data, the accuracy of the predicted strength is within 17%.

References

[1] Caminero MA, Pavlopoulou S, Lopez-Pedrosa M, Nicolaisson BG, Pinna C, Soutis C. Analysis of adhesively bonded repairs in composites: Damage detection and prognosis. Compos Struct 2013;95:500–17.

[2] Caminero MA, Lopez-Pedrosa M, Pinna C, Soutis C. Damage monitoring and analysis of composite laminates with an open hole and adhesively bonded repairs using digital image correlation. Compos Part B Eng 2013;53:76–91.

[3] Bouzgou AA, Tati A, Khechai A. Analysis of deflection in isotropic and orthotropic rectangular plates with central opening under transverse static loading. Appl Mech Behav Mater Eng Syst 2017:399–409.

[4] Bouzgou AA, Khechai A, Tati A. Stress concentration and deflection in isotropic and orthotropic plates with opening finite element study. Revue des Compos et des Matériaux Avancés (Editions Hermes/Lavoisier) 2015;25(3–4):385–405.

[5] Khechai A, Tati A, Guettala A. Finite element analysis of stress concentrations and failure criteria in composite plates with circular holes. Front Mech Eng 2014;9(3):281–94.

[6] Louhghalam A, Igusa T, Park C, Choi S, Kim K. Analysis of stress concentrations in plates with rectangular openings by a combined conformal mapping–finite element approach. Int J Solids Struct 2011;48(13):1991–2004.

[7] Muskhelishvili NI. Some basic problems of the mathematical theory of elasticity. Springer Science & Business Media; 2013.

[8] Ukadgaonker VG, Rao DKN. A general solution for moments around holes in symmetric laminates. Compos Struct 2000;49(1):41–54.

[9] Ukadgaonker VG, Rao DKN. A general solution for stresses around holes in symmetric laminates under inplane loading. Compos Struct 2000;49(3):339–54.

[10] Ukadgaonker VG, Rao DKN. A general solution for stress resultants and moments around holes in unsymmetric laminates. Compos Struct 2000;49(1):27–39.

[11] Rao DKN, Babu MR, Reddy KRN, Sunil D. Stress around square rectangular cutouts in symmetric laminates. Compos Struct 2010;92(12):2845–59.

[12] Savin GN. Stress concentration around holes. Pergamon Press; 1961.

[13] Rezaeepazhand J, Jafari M. Stress analysis of perforated composite plates. Compos Struct 2005;71(3):463–8.

[14] Wu G, Tan Y, Yang JM. Evaluation of residual strength of notched fiber metal laminates. Mater Sci Eng A 2007;457(1):338–49.

[15] Awerbuch J, Madhukar MS. Notched strength of composite laminates: predictions and experiments- a review. J Reinf Plast Compos 1985;4(1):3–159.

[16] Whitney JM, Nuismer RJ. Stress fracture criteria for laminated composites containing stress concentrations. J Compos Mater 1974;8(3):253–65.

[17] Hwan CL, Tsai KH, Chiu CH, Huang YS. Strength prediction of woven hybrid composite laminates each with a center hole. J Compos Mater 2014;48(13):1637–44.

[18] Kamala Kannan V, Murali V, Rajadurai A, Nageswara Rao B. Tension and compression strength evaluation of composite plates with circular holes. J Reinf Plast Compos 2010;29(10):1500–14.

[19] Hwan CL, Tsai KH, Chiu CH, Huang YS. Strength prediction of braided composite plates with lateral holes by a finite element-based point stress criterion. J Compos Mater 2013;47(9):1161–8.

[20] Pipes RB, Wetherhold RC, Gillespie Jr JW. Notched strength of composite materials. J Compos Mater 1979;13(2):148–60.

[21] Kim JK, Kim DS, Takeda N, strength Notched, hole fracture criterion in fabric composite plates containing a circular. J Compos Mater 1995;29(7):982–98.

[22] Kannan VK, Murali V, Rajadurai A, Rao BN. Finite element analysis and notched tensile strength evaluation of center-hole 2d carbon/carbon laminates. Adv Compos Mater 2011;20(3):289–300.

[23] Khechai A, Tati A, Guettala A. Numerical study of the effect of presence of geometric singularities on the mechanical behavior of laminated plates. J Inst Eng (India): Ser C 2017:1–12.

[24] Rudan S, Garbatov Y, Soares CG. Finite element study of stress concentration factors in ship knuckle details. In: 3rd International Congress of Croatian Society of Mechanics, 2000.

[25] Flament C, Salvia M, Berthel B, Crosland G. Local strain and damage measurements on a composite with digital image correlation and acoustic emission. J Compos Mater 2016;50(14):1989–96.

[26] Mbarek TB, Robert L, Hugot F, Orteu JJ. Mechanical behavior of wood–plastic composites investigated by 3d digital image correlation. J Compos Mater 2011;45(26):2751–64.

[27] Kureemun U, Ridha M, Tay TE. Biaxial tensile-compressive loading of unnotched and open-hole carbon epoxy crossply laminates. J Compos Mater 2015;49(23):2817–37.

[28] Blaber J, Adair B, Antoniou A. Ncorr: open-source 2D digital image correlation matlab software. Exp Mech 2015;55(6):1105–22.

[29] Pierron F, Green B, Wisnom MR. Full-field assessment of the damage process of laminated composite open-hole tensile specimens. Part I: Methodology. Compos Part A Appl Sci Manuf 2007;38(11):2307–20.

[30] Pierron F, Green B, Wisnom MR, Hallett SR. Full-field assessment of the damage process of laminated composite open-hole tensile specimens, Part II: Experimental results. Compos Part A Appl Sci Manuf 2007;38(11):2321–32.

[31] Lagattu F, Lafarie-Frenot MC, Lam TQ, Brillaud J. Experimental characterisation of overstress accommodation in notched cfrp composite laminates. Compos Struct 2005;67(3):347–57.

[32] Grediac M. The use of full-field measurement methods in composite material characterization: Interest and limitations. Compos Part A Appl Sci Manuf 2004;35(7):751–61.

[33] Caminero MA, Pavlopoulou S, López-Pedrosa M, Nicolaisson BG, Pinna C, Soutis C. Using digital image correlation techniques for damage detection on adhesively bonded composite repairs. Adv Compos Lett 2012;21(2):51–7.

[34] Konish HJ, Whitney JM. Approximate stresses in an orthotropic plate containing a circular hole. J Compos Mater 1975;9(2):157–66.

[35] Ahmed KS, Vijayarangan S, Naidu ACB, properties Elastic. notched strength and fracture criterion in untreated woven jute–glass fabric reinforced polyester hybrid

composites. Mater Design 2007;28(8):2287–94.
[36] Potti PKG, Rao BN, Srivastava VK. Notched strength evaluation of fabric laminates having a circular hole. Adv Compos Mater 2000;9(1):47–58.
[37] Tan SC. Finite-width correction factors for anisotropic plate containing a central opening. J Compos Mater 1988;22(11):1080–97.
[38] Hecht F. New development in Freefem + +. J Numer Math 2012;20(3–4):251–66.
[39] Zienkiewicz OC, Taylor RL. The finite element method: solid mechanics. Butterworth-heinemann 2000.
[40] ASTM. Committee D-30 on composite materials. standard test method for tensile properties of polymer matrix composite materials. ASTM International; 2008.
[41] ASTM Committee. Standard test method for in-plane shear response of polymer matrix composite materials by tensile test of a ± 45 laminate ASTM D 3518/D 3518; 2001.
[42] Chien CH, Su TH, Wang CT, Chen BS. Using digital image correlation method for measuring residual stress in the nickel coating of the specimen. Exp Tech 2015.
[43] Ben-Israel Adi. A newton-raphson method for the solution of systems of equations. J Math Anal Appl 1966;15(2):243–52.
[44] Tercan M, Asi O, Aktaş A. Determination of the critical crack length of notched weft-knitted glass fiber variable width composite plates. Compos Struct 2007;77(1):111–9.
[45] Dirikolu MH, Aktaş A. Analytical and finite element comparisons of stress intensity factors of composite materials. Compos Struct 2000;50(1):99–102.
[46] Hwang WJ, Park YT, Hwang W. Strength of fiber reinforced metal laminates with a circular hole. Met Mater Int 2005;11(3):197–204.
[47] Tinô SRL, Fontes RS, de Aquino EMF. Theories of failure average stress criterion and point stress criterion in notched fiber-reinforced plastic. J Compos Mater 2014;48(21):2669–76.